THE MORPHOLOGY OF POLYMER MODIFIED ASPHALT AND ITS RELATIONSHIP TO RHEOLOGY AND DURABILITY

A Thesis

by

ZACHARY ROTHMAN KRAUS

Submitted to the Office of Graduate Studies of
Texas A&M University
in partial fulfillment of the requirements for the degree of

MASTER OF SCIENCE

August 2008

Major Subject: Chemical Engineering

THE MORPHOLOGY OF POLYMER MODIFIED ASPHALT AND ITS RELATIONSHIP TO RHEOLOGY AND DURABILITY

A Thesis

by

ZACHARY ROTHMAN KRAUS

Submitted to the Office of Graduate Studies of
Texas A&M University
in partial fulfillment of the requirements for the degree of

MASTER OF SCIENCE

Approved by:

Chair of Committee,	Charles J. Glover
Committee Members,	Mariah Hahn
	Lale Yurttas
	Amy Epps Martin
Head of Department,	Michael Pishko

August 2008

Major Subject: Chemical Engineering

ABSTRACT

The Morphology of Polymer Modified Asphalt and Its Relationship to Rheology and Durability.

(August 2008)

Zachary Rothman Kraus, B.S., Georgia Institute of Technology

Chair of Advisory Committee: Dr. Charles J. Glover

Polymers are added to asphalt binders primarily to stiffen the binder at higher temperatures and thus to protect the pavement against rutting at summertime temperatures early in the pavement's life. Also, it has been noted that polymers typically increase the ductility of a binder and that some polymer-asphalt combinations are especially effective. Furthermore, it is hypothesized that enhancing a binder's ductility, and maintaining this enhancement with binder oxidative aging, contributes to enhanced binder durability in pavements. However, polymer-asphalt interactions and how they might contribute to improved binder performance is not well understood. The goal of this work was to probe the relationship of polymer morphology on asphalt binder rheology and mixture durability.

Experiments were conducted on asphalt mixtures and binders, and as a function of oxidative aging. PFC mixtures, which are an open mixture designed to allow enhanced water drainage, were of specific interest. These mixtures were tested for Cantabro Loss, an indicator of a mixture's likelihood of failure by raveling. Asphalt binders were tested using dynamic shear rheometry (DSR), which provided the DSR function, (G'/(η'/G'), a measure of binder stiffness that includes both the elastic modulus and the flow viscosity), ductility (used to measure the elongation a binder could withstand before failure), gel permeation chromatography (GPC), used to estimate the relative amount of polymer) and fluorescence microscopy (used to image the polymer morphology in the asphalt binder).

From these data, relationships were assessed between binder morphology and binder rheology and between binder rheology and mixture durability, all as a function of binder oxidative aging. Polymer morphology related to ductility enhancement. Polymer morphology related to a change in the DSR function, relative to the amount of polymer, as measured by the polymer GPC peak height. Cantabro loss correlated to the DSR function (R^2=0.963). The overall conclusion is that polymer morphology, as indicated by fluorescence microscopy, relates to both the rheological properties of the binder and the Cantabro loss of the mixture. These relationships should yield a better understanding of polymer modification, increased mixture durability (decreased raveling) and improved rheological properties (DSR function and ductility).

TABLE OF CONTENTS

LIST OF FIGURES

FIGURE Page

LIST OF TABLES

CHAPTER I
INTRODUCTION

Polymer modification is added to asphalt binders to improve the rheological properties of the binder which can affect mixture durability. At placement, the polymer improves the stiffness of the binder, which stiffens the mixture and helps prevent rutting. Later the polymer's ductility enhancement is hypothesized to improve the durability to cracking in dense mixtures.

For permeable friction courses (PFC), there are currently no binder rheological properties to predict the long term durability of the mixture. PFCs differ from dense mixtures because of their open mixture design and ability to remove water from the surface of the asphalt mixture. PFCs most common form of failure is raveling which is believed to relate to the stiffness of the binder which can be measured using rheological instruments.

These rheological measurements should provide a possible estimate of the durability for PFC mixtures. Polymer modified binders are typically used for PFC mixtures. Sometimes the polymer modifier does little to enhance the ductility of the unmodified binder. The best method to understand what causes this lack of ductility improvement is microscopy which allows the polymer's microscopic two phase system to be viewed in the asphalt binder. Combining these two separate problems (ductility affecting PFC durability and polymer morphology related to rheology) into one larger problem (polymer morphology affecting rheology and PFC durability) is the main goal of this thesis.

To accomplish this goal, these two problems are discussed throughout the text, as separate issues. One issue, possible relations of polymer morphology to rheology is discussed in Chapter II. The other issue, rheology properties affecting PFC durability, is discussed in Chapter III. Only in Chapter IV, the conclusion, are the two problems reunited as a solution for the main goal of this thesis.

This thesis follows the style of *Transportation Research Record.*

BACKGROUND

The history of Porous Friction Course (PFC) and microscopy is fairly new. Each has had its unique problems and uses during its history. These problems and uses are explained in subsequent sections. The first section is on how binder rheology may be used to decrease raveling in PFC mixtures. The second section is on how microscopic properties of polymer may affect binder rheology.

Using Binder Rheology to Decrease Raveling of Mixture Designs

The history of PFC mixes in the United States of America (U.S.A.) is about 60 years old. PFCs were primarily implemented to improve wet weather driving and reduce noise. The wet weather improvements and reduced noise occur because of the open nature of the asphalt mixture. Open graded asphalt allows water to drain away from the surface which decreases splash and spray, increases wet weather friction, and reduces hydroplaning. In 1974, the Federal Highway Administration (FHWA) developed a PFC mixture design. This mixture design was used by several states but then discontinued by many of them because of performance issues (*1*). These issues are raveling, and draindown (*2*). A survey done by the National Center for Asphalt Concrete in 1998 showed states using PFC were using polymer modified asphalt and a different gradation than that recommended by the FHWA. These states have an average service life of ten years for their PFC mixtures (*3*). From the above facts, a good design yields better service life and fewer durability issues for PFC mixtures.

Designing a good PFC is a multistep process. The first step is selecting the proper binder. The second step is selecting the aggregate and gradation. If filler will be used, the third step is deciding on which filler. The fourth step is selecting the film thickness/asphalt content. The fifth step is to select the void content. The sixth step is testing the draindown, permeability and resistance to abrasion of the designed mixture. If the final mixture does not meet the test requirements, the mix is remade with new

specifications. Many laboratories, in an effort to find the best mixture design, usually test a combination of binder choice, aggregate design, filler selection and film thickness.

Although all of these design steps are important, the binder selection can be the most effective at changing the resistance to abrasion. In a report by Kandhal and Mallick, Cantabro (resistance to abrasion) experiments on PFC mixtures made with PG 64-22, PG 64-22 SBS (styrene-butadiene-styrene), PG 76-22 SB (styrene-butadiene), PG 64-22 CF (Cellulose fiber) and PG 76-22 SB-SW (Slag wool) were all made with the same gradation, asphalt content and air voids (*1*). The percent loss for the PG 64-22 and PG 76-22 SB mixture were 26.2 percent and 15.7 percent respectively. The stiffer PG 76-22 reduces the loss of material in the Cantabro test by approximately 10 percentage points more than that for the PG 64-22. When slag wool is added to the PG 64-22 and PG 76-22 mixtures, the Cantabro loss is 19.3 percent and 9.0 percent respectively. The added slag wool decreases the Cantabro loss in both mixture designs by about 7 percentage points compared to the binder with no filler (*1*). These data show that binder type can have a more significant effect on the abrasion resistance than filler type.

In an experiment done by Hassan, mixtures were made using penetration grade 60-70 binder with or without styrene butadiene rubber (SBR) (*4*). These mixture designs had a binder content ranging from 4.5 percent to 6.5 percent and were tested in an unaged state and aged state with the Cantabro test. The aged state was produced in an oven at 60 °C for seven days. Whether these aged samples were aged in a mixture form or in the loose state is not known. For the unaged Cantabro test, the unmodified binder mixture had approximately 60 percent loss at 4.5 percent binder content, and the SBR binder mixture had approximately 50 percent loss at 4.5 percent binder content and approximately 10 percent loss at 6.5 percent binder content. These numbers show in the unaged state, at the 6.5 percent binder content, the polymer added to the binder decreases the percentage loss in the Cantabro test by 30 percentage points. For the aged Cantabro test, the unmodified mixture had 100 percent loss at 4.5 percent binder content and approximately 90 percent loss at 6.5 percent binder content, and the SBR binder mixture had approximately 60 percent loss at 4.5 percent binder content and approximately 40

percent loss at 6.5 percent binder content. These results for the aged mixes show the polymer decreases the Cantabro loss by 40 percentage points at 4.5 percent binder content and 50 percentage points at 6.5 percent binder content (*4*). Again, the data show that utilizing a different binder may have an enormous effect on the Cantabro loss. Also, once the binder with the lowest Cantabro loss is chosen, adding filler can improve the mixture design further.

The resistance to abrasion is a simulated measurement of raveling which is the most common source of PFC failure. Raveling occurs when the aggregate falls from the binder matrix and is caused by stiffening of the asphalt binder due to oxidative aging (*5*). Rheological tests could be utilized to analyze binder stiffness with aging and then these results could be correlated to the Cantabro loss (Resistance to Abrasion). Unfortunately this correlation will not be exact but an estimate of the Cantabro loss, because rheological tests do not take into account binder adhesive properties to fillers and aggregate. Even though rheological tests may only give approximate Cantabro Loss values, rheological tests could still be used as a tool for acquiring an estimate of the mixture's Cantabro Loss.

There are many rheological tests done on asphalt binders which could be used for binder selection including ductility/force ductility, dynamic shear rheometer (DSR), viscometer, and bending beam tests. Of all of these tests, DSR is an easy test to run because it takes less than an hour and gives a lot of information: G' (dynamic storage modulus), G" (dynamic loss modulus), G* (dynamic complex modulus), η' (dynamic viscosity response), η" (dynamic out-of-phase viscosity), η* (dynamic complex viscosity), δ (phase angle).

Ductility (measurement of binder's elongation) at 15 °C, 1 cm/min has been shown to relate to cracking failure. Ruan et. al. showed that DSR results correlate with ductility below 10 cm according to

$$\text{ductility} = 0.23 * (G'/(\eta'/G')^{(-0.44)} \qquad (1\text{-}1),$$

where G' is the dynamic storage modulus and η' is the dynamic viscosity response reported at 10 °C and 0.005 s^{-1} (*6*). Because ductility has been shown to relate to

cracking failure in pavement, it has been hypothesized that DSR can be used to estimate both ductility and the likelihood of cracking failure in pavement (*6*). The Strategic Highway Research Project (SHRP) used G*/sin δ at 10 rad/s to estimate rutting performance (*7*).

Microscopic Effects of Polymer Modification on Asphalt Rheology

In the previous section, the background of PFC and the possible relationship between rheology and PFC durability was explained. In this next section, background information on polymer modified asphalts, microscopy, and their effects on rheology is given. These two backgrounds are related through rheology. This relationship is important because by improving the polymer modified asphalt's rheology; the durability of PFCs could be improved.

In this thesis, SBS is considered because it is the most commonly used polymer modifier for asphalt (*8*). Poly (styrene-butadiene-styrene) (SBS) is a tri-block polymer with a butadiene block in the middle of two styrene blocks (*7*). The blocks form a two-phase morphology. The polystyrene blocks form the hard, glassy phase which increases rutting resistance and the butadiene blocks form the soft, rubbery phase which increases thermal cracking resistance (*9, 10*). The polystyrene blocks can physically crosslink to form a network with elastic properties (*7*). SBS added to asphalt binder forms two phases, a polymer rich phase and an asphalt rich phase. The polymer rich phase swells as it absorbs aromatics from the asphalt (*11*).

Because the polymer forms microscopic phases in the asphalt binder, one way to discover what happens to SBS with aging is to use microscopy. Techniques that have been used for asphalt research are scanning electron microscopy (SEM), Atomic Force Microscopy (AFM), tunneling electron microscopy (TEM), confocal laser scanning microscopy (CLSM), environmental electron scanning microscopy (ESEM), cryo-scanning electron microscopy (CSEM) and fluorescence microscopy (*11-16*). Scanning electron microscopy has poor resolution with oily substances such as asphalt binder. To

solve the resolution problem, the samples are deoiled and then metallized. This process causes a volume change to take place and in some samples fissures are formed. AFM has problems with the tip sticking to the asphalt. Also AFM needs nearly smooth surfaces to operate otherwise the cantilever will begin to oscillate (*12*). Environmental scanning electron microscopy has limited resolution. Cryo-scanning electron microscopy is conventional SEM at -165° C. The cold temperature allowed viewing of soft specimens like asphalt, but the resolution is low or medium. Also the sample still requires a metal coating (*11*). Asphalt was found to be electron beam sensitive and tended to form cracks with prolonged exposure (*13*). Fluorescence CLSM is similar to reflective fluorescence microscopy. The difference is fluorescence CLSM uses laser beams and reflective fluorescence microscopy uses a UV lamp or an arc lamp. Champion et al. realized Rhodamine-B and other stains were not needed because the SBS swells from the aromatic species in asphalt which fluoresce (*11*). Fluorescent microscopy is good for seeing the microstructures in asphalt which range from 10 to 100 µm (*15*). Although fluorescence microscopy and CLSM are similar, for this work fluorescence microscopy was a better choice because of the availability of the equipment.

Asphalt binder contains aromatic rings that are important to fluorescence. The aromatic rings by themselves do not cause fluorescence but if electron donating groups or electron accepting groups, shown in Table 1-1, are added to the ring structure fluorescence may occur. If an electron donating group and an electron acceptor group are attached to a benzene ring ortho or para to each other, fluorescence will occur. In a condensed ring system, if a conjugated bond path can form between the electron donating and electron accepting group, fluorescence will occur. Also, if two terminal oxygen or nitrogen atoms on or in the aromatic structure are able to form resonance structures, fluorescence will be highly likely.

TABLE 1-1 Electron Donor and Electron Acceptor Groups (*17*)

Electron Donor Groups	Electron Acceptor Groups
Amino	Cyano
Alkylamino	Carbonyl
Dialkylamino	Vinylene
Oxido	Styryl
Hydroxy	Acrylic Ester
Alkoxy	β-methacrylic ester
	Benzoxazolyl
	Benzothiazolyl
	Benzimidazolyl

Although in normal light asphalt looks black, under a fluorescence microscope, it fluoresces green. The fluorescence of the unmodified binder occurs from some of the thousands of compounds in the unmodified binder in which the chemical structure follows the rules described above. The fluorescence microscope differs from a normal light microscope because two filters and a dichromatic mirror are attached to the fluorescence microscope. The two filters and dichromatic mirror are part of a set that changes the source light to the excitation frequency and allows the fluorescence emissions to go to the eyepiece (*18*).

Based on the above rules of fluorescence, brightness theoretically speaking could be used as a measure of hardening susceptibility and a measurement of asphalt compatibility. The hardening susceptibility is:

$$HS = \frac{d \log_{10} \eta^*_{60\deg C}}{dCA}.$$

This relationship shows that log viscosity at 60 °C increases linearly with carbonyl area increases, due to oxidative aging and measured by infrared spectroscopy. The above derivative can be split into two derivatives

$$HS = \frac{d \log_{10} \eta^*_{60 \deg C}}{dCA} = \left(\frac{d \log_{10} \eta^*_{60 \deg C}}{d\%A} \right) \left(\frac{d\%A}{dCA} \right),$$

where d%A is the change in asphaltene in the asphalt (*19*). The other theory is that only the polar aromatics and napthene aromatics fluoresce when separated from the asphalt binder (*16*). Therefore as polar and napthene aromatics change to asphaltenes with oxidative aging, the brightness would decrease. This brightness decrease would correspond to the increase in asphaltene with carbonyl area leading to a graph that looks like a chart for hardening susceptibility. To produce a compatible SBS modified asphalt, the aromatic portion should be high and the asphaltenes should be less then 6 percent by weight (8, 15). Using the concept that only the polar aromatic and napthene aromatic portion of the asphalt binder fluoresce, a brighter unmodified binder should yield a better SBS modified binder (*16*).

To summarize, in the first background section, it was noted that sing a polymer modified asphalt was found to improve PFC durability. Also, the choice of binder was shown to have a larger impact on durability than the choice of filler. Binder rheological tests, such as DSR, force ductility, and ductility, are believed to be related to PFC durability tests because they show the stiffness of the binder with oxidative aging. In the second section of this background, it was noted that the morphology of the SBS forms a two phase system in asphalt. This two phase system can be seen using microscopy. The two best microscopes for examining this two phase system are a fluorescence microscope and a CLSM. The fluorescence in the asphalt is caused by the many aromatic compounds in the asphalt. The fluorescence brightness is believed to correspond to the concentration of the polar aromatics and napthene aromatics in the asphalt. A SBS compatible asphalt should have a high concentration of the aromatics (napthene and polar) in the asphalt. Therefore, a brighter asphalt image is hypothesized to relate to a more compatible SBS modified binder.

OBJECTIVES

The PFC and Microscopy sections above were discussed as distinctly different topics. The PFC section concentrated on binder selection issues for designing a better PFC. The microscopy section discussed how microscopic behavior may affect macroscopic properties. These two sections are explained further in the following paragraphs as they relate to each other.

Using DSR to Predict Raveling of PFC Mixture Designs

The dynamic shear rheometer (DSR) should be used to prescreen for PFC mixtures. This prescreen selection test would save lots of time designing these mixtures. Currently, combinations of both the different binders and all the mixture design elements must be tested. If one of these factors could be removed from the mixture design process, the process could be finished faster. The most likely candidate to remove from the mixture design process is binder selection. Currently there are many tests to analyze binder and future mixture properties. DSR is an extremely fast test and has been shown to predict future mixture properties (rutting and cracking) (6, 7); therefore, it would be an ideal prescreen for PFC mixtures.

The mixture property to be predicted in PFC is the amount of raveling of the mixture with aging. Raveling is the most common form of PFC failure. Raveling causes the mixture to degrade by losing aggregate (*3*). Raveling is tested for each mixture during the design process and mixtures must fall below a certain aggregate loss percent to be even considered for a final mixture design. The DSR should be used to predict the amount of raveling of the mixture in the unaged state and the aged state. If the effect of the binder on raveling could be predicted from the DSR before making the mixture, each binder would not need to be tested in the mixture, thus saving time, energy, and money.

Using Microscopy to Relate Polymer Morphology to Asphalt Binder Rheology

Polymer is added to asphalt binder to improve the rheological properties (*20*) such as ductility, G*, and δ. Force ductility curves (stress versus elongation) of polymer modified asphalts initially show two distinct regions of stress increase with elongation shown in Figure 1-1. The first linear region has been termed the asphalt modulus and the second linear region the asphalt-polymer modulus. The asphalt modulus results from the interactions of the asphalt components and is present in all asphalts. The asphalt-polymer modulus is thought to arise from asphaltene and polymer interactions and uncoiling of polymer chains. As the polymer modified asphalt ages the asphalt-polymer modulus disappears, lowering the asphalt ductility significantly. Eventually the ductility enhancing effects of the polymer disappear altogether and the ductility values of polymer modified binders match much more closely the ductility values of the unmodified binders (*21*).

DSR results also show the same decrease in polymer effectiveness with aging through measurement of different variables, G* and δ. G* is the complex dynamic shear modulus and is composed of G', the storage modulus, and G", the loss modulus. δ is a measure of the visco-elasticity and is defined by tan δ = G"/G'. At δ equal to 90 degrees, the material is purely viscous, while at δ equal to 0 degrees, the material is purely elastic. At high temperature or low frequency, polymer modification increases G* relative to the unmodified binder, improving the rutting resistance. Polymer modified binders show a decrease in loss tangent compared to unmodified binder at high temperature or low frequency, which corresponds to an increase in the elasticity of the material. The loss tangent curve shows the existence of a polymer network if the loss tangent master curve contains a plateau region. With aging, a polymer modified asphalt's low frequency G* increases and the loss tangent decreases, showing an increase in the elasticity of the material at a given frequency. Also, with aging, polymer networks become damaged, destroying/decreasing the plateau region (*21*).

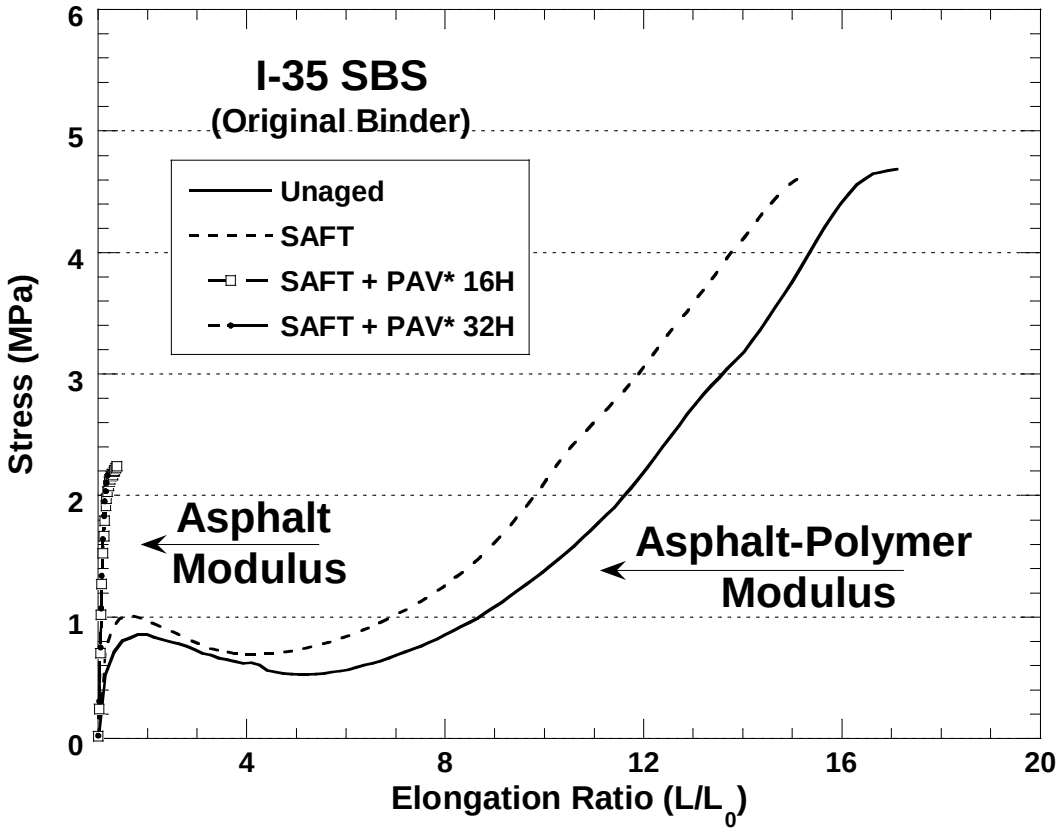

FIGURE 1-1 A Force Ductility Plot Showing the Asphalt Modulus and Asphalt-Polymer Modulus

Force ductility data show with increased aging that the polymer loses its effectiveness in improving the ductility. DSR results exhibit evidence that the polymer networks are being damaged from aging. Interestingly, with aging, the polymer modified asphalt still contains polymer as measured by gel permeation chromatography/size exclusion chromatography (GPC/SEC) (*21*). The observations from force ductility and DSR demonstrate that the polymer modified asphalt is initially a very good way to improve an asphalt binder. But with aging, the added polymer makes little to no difference in ductility properties.

The above results lead to the hypothesis that changes in the polymer morphology within the binder are affecting the results from the rheological tests: force ductility, DSR and ductility. A good way to examine the polymer morphology is through the use of

microscopy. The images from microscopy should give a clearer understanding of the role the polymer plays in the observed rheological changes.

The objective of this thesis is to investigate the rheological and morphological changes that lead to changes in a polymer modifier's effectiveness and to changes in PFC durability with oxidative aging. With an understanding of that fundamental mechanism, better polymer modified asphalts can be produced.

CONCLUSIONS

This proposed project should effectively discover the mechanism that leads to polymer modified asphalts performing like unmodified asphalts after aging. Also this proposed project should enable the asphalt community to better understand Cantabro Loss using DSR measurements. Both of these proposed objectives are new, and any results will lead to a better understanding of asphalts.

CHAPTER II
MICROSCOPIC EFFECTS OF POLYMER ON ASPHALT RHEOLOGY

BACKGROUND

In Chapter I, the ductility enhancement that can result from polymer modification was introduced. However, such enhancement is not automatic. In this chapter we will discuss two polymer modified binders, one with very little ductility improvement and the other with exceptional ductility improvement. By examining these two binders it was hoped to gain greater insight to the mechanism by which SBS modifier increases ductility.

SPECIFIC PROBLEM

During the TxDOT 0-4688 project, two SBS modified binders showed different degrees of ductility enhancement at PAV* aging levels over their PG 64-22 unmodified binders. These two unmodified binders were the Koch PG 64-22 and the Alon PG 64-22. The Alon PG 64-22 modified binders showed the most ductility enhancement and the Koch PG 64-22 modified binders showed the least ductility enhancement. The Koch PG 64-22, Alon PG 64-22, and their modified binder's ductility versus DSR properties are shown in Figure 2-1 (*22*).

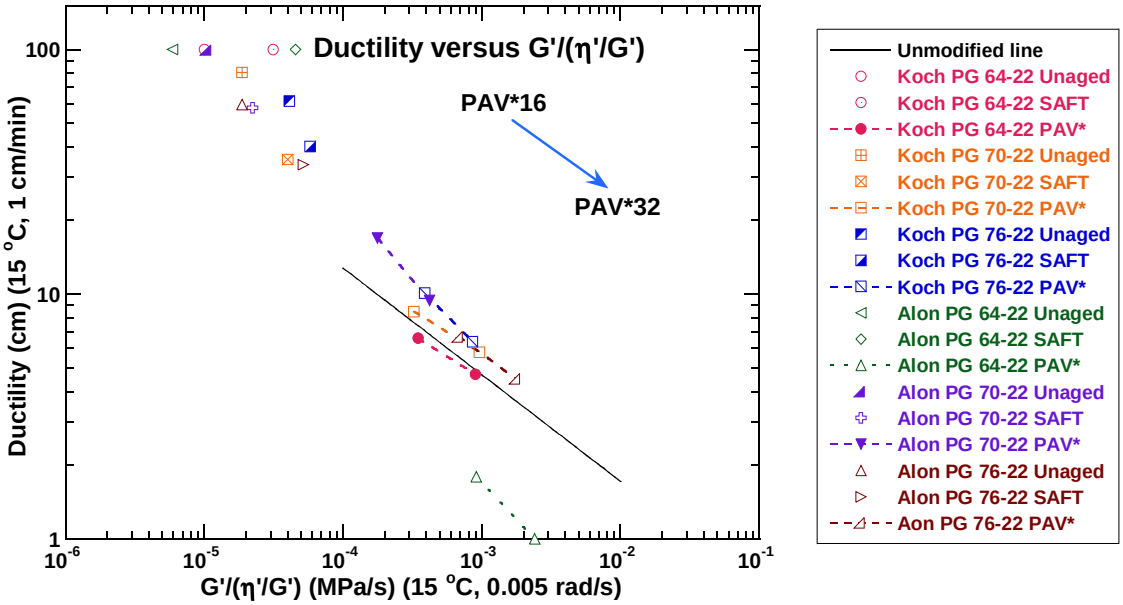

FIGURE 2-1 Ductility Versus DSR Function Plot Showing the Polymer's Effect on Ductility Enhancement (22)

Figure 2-1 shows ductility enhancement from adding polymer to the Koch PG 64-22 and Alon PG 64-22 base binders. Ductility enhancement is the ability of the added polymer to increase the ductility of the base binder compared to the unmodified binder line. Ductility enhancement can better be understood by a quick examination of Equation 2-1:

$$DE = \Delta D_M - \Delta D_U, \quad (2\text{-}1)$$

where DE is the ductility enhancement, ΔD_M is the difference between the modified binder's ductility and the ductility on the unmodified line below or above the modified binder, and ΔD_U is the difference between the unmodified binder's ductility and the ductility on the unmodified line above or below the unmodified binder. The values of $\Delta D_{M \text{ and}} \Delta D_U$ are negative if the point lies below the line.

The unmodified binder line in Figure 2-1 comes from a relationship discovered by Ruan et al. (*6*). This relationship showed that the ductility of an unmodified binder

below 10 cm was affected by its DSR Function. Equation 1-1 describes this relationship and is the equation used to plot the unmodified binder line (*6*).

Examining Figure 2-1 using the ductility enhancement measure, the Alon binders at PAV* aging levels are out performing the Koch binders shown in Table 2-1. The PAV* Alon PG 76-22 have approximately 6 cm of ductility enhancement. The Alon PG 70-22 PAV* 16 and PAV* 32 binders have 5 and 6 cm respectively of ductility enhancement. The Koch PG 70-22 PAV*16 and PAV*32 binders show a ductility enhancement of 2 cm and 1 cm respectively. The Koch PG 76-22 PAV*16 and PAV*32 binders were found to have a ductility enhancement of 3.5 cm and 2 cm approximately. The Alon binders have between 2 to 6 times the amount of ductility enhancement as the Koch binders at PAV* aging levels. The big question to ask is why these two binders are behaving so differently. (It should be noted, however, that the Along base binder starts at unusually low ductilities at these aging levels.)

TABLE 2-1 Ductility Enhancement of Koch and Alon Polymer Modified Binders

	Ductility Enhancement (cm) $(\Delta D_M - \Delta D_U)$	
	PAV*16	PAV*32
Alon PG 70-22(S)	5	6
Alon PG 76-22(TS)	6	6
Koch PG 70-22(S)	2	1
Koch PG 76-22(S)	3.5	2

To answer this question the binders in Figure 2-1 were examined using the following techniques:

- GPC
- DSR
- Fluorescence Microscopy
- Force Ductility
- Ductility.

METHODOLOGY

In this section, rheology and GPC are related to microscopy images. The DSR, ductility, and force ductility measure rheological properties that change with aging. These rheological properties are compared to the microscopy images. The GPC is used to indicate the apparent amount and molecular size of the polymer in the microscopy images. The rheology, GPC and microscopy data are compared to determine a possible qualitative relation between them, designed to address four questions: Why does the asphalt-polymer modulus in the force ductility data disappear with aging? Why does the plateau region in the loss tangent master curve decrease or cease to exist upon oxidative aging? Why, with enough aging, do the ductility values of polymer modified asphalt decrease to match the ductility values of the base asphalt? Why, when the asphalt loses the polymer related properties of enhanced ductility, asphalt-polymer modulus and the plateau region, is there still polymer in the asphalt binder? The experiments are outlined below.

Four levels of aging were used in these two investigations: unaged, SAFT, PAV*16 and PAV*32. Seventy grams of the unaged, and SAFT, PAV*16 and PAV*32 asphalt are needed for further testing. To acquire the SAFT, PAV*16 and PAV* 32 asphalt, two 250 g batches of asphalt were SAFT aged. The SAFT aging procedure is to stir 250 g of asphalt binder in an air flow vessel at 325° F (163° C) for 35 minutes while air is being blown into the asphalt. The stirring was done at 700 RPM and the air flow

rate was 2000 mL/min. After SAFT, 170 g of SAFT aged binder was PAV* aged. To do the PAV* test 17 g of asphalt was melted into a PAV pan to form a 1 mm thick layer. The pressure and temperature of the PAV* test are 2.2 MPa and 90° C. The PAV*16 procedure needed 10 pans and lasted 16 hours. After the PAV*16 aging is finished, five of the PAV*16 pans continued to be aged for another sixteen hours using the PAV* aging conditions. These two PAV* aging steps produced 75 g of PAV*16 and PAV*32 asphalt binder. These four levels of aging allowed lab testing on binders aged up to the equivalent of 6 years in the pavement (*22*).

The force ductility test was conducted at 4 °C with an extension rate of 1 cm/min. The initial sample has a gauge length of 3 cm and a uniform cross section in the middle of 1 cm by 0.5 cm. The force ductility test measures force as a function of extension ratio.

The ductility test was conducted at 15 °C with an extension ratio of 1 cm/min. The initial sample has a gauge length of 3 cm and a tapered cross section. The ductility measures the maximum extension of the binder (*22*). Although ductility and force ductility do not give as much information or the same type of information as the DSR, Ductility and force ductility still measure the effect of binder stiffness on the asphalt's ability to elongate without failure.

The DSR test was done using a Carri-Med CSL500 dynamic shear rheometer. Enough sample of asphalt was applied to the test surface to fill the gap between the surface and the plate after the 2.5 cm plate squeezed the sample. The gap size used was 500 µm. The excess sample then was scraped away. The three testing methods were carried out at 44.7 and 60 °C. The first test was at 60 °C and used frequencies from 0.1 to 100 rad/s. The second test decreased the temperature from 60 °C to 44.7 °C and was conducted at10 rad/s. A curve was created from the 60 °C DSR test. The 44.7 °C data gives G' and G" which is used to calculate η' (22). These G' and η' values correlate to the ductility from Equation 1. These two testing methods will give a very broad view of the rheology of the asphalt binder being tested.

GPC was used to detect the presence of polymer. To run the GPC, 10 mL of THF was added to 0.2 g of asphalt binder sample in a 20 mL vial. The mixture was then filtered through a 0.45 µm syringe filter and placed in a vial. The machine was then run using the samples in the vials (*22*).

To make the fluorescence microscopy slides, the asphalt samples were heated in an oven between 300 °F (149 °C) and 315 °F (157 °C) for 8 to 25 minutes depending on the sample becoming molten. Once the sample was molten, a slight amount of the sample was poured onto a marked slide. Another slide will be immediately placed on top and the top slide was pressed down until the asphalt would not squeeze anymore under light pressure. Since we used very thin slides, heavy pressure can not be applied because the slide would break. Ten pictures of the sample were taken using 50x, 100x and 200x settings. The exposure for these pictures was set using the automatic exposure meter on the microscope. Each photo, except two, should be at different locations on the sample (*22*).

Before the photos could be analyzed, the original images needed to be enhanced to increase the visual contrast between the asphalt and the polymer phases. The enhancement process was done on GIMP which is a free imaging program (*23)*. The software assigns values for brightness, and for the colors red, green and blue on a 0 to 255 scale. In addition, there is a functionality called levels. The levels function requires two assigned values between 0 and 255. The function changes all numbers below the low assigned value to a value of 0 and all numbers above the high assigned value to a value of 255. In between the two assigned values, the values change from 0 to 255 based on the gamma value. A gamma value of 1 makes the change from 0 to 255 a gradual change. A gamma value of 0.1 creates an instantaneous change of all values below the high assigned value to be 0. A gamma value of 10 creates the exact opposite change: all values above the low assigned value are now 255.

To enhance the microscopy images, the level function was used with gamma set to 1 and the assigned values set from the brightness curve. The brightness curve consists of the 0 to 255 scale on the x axis and the number of pixels assigned with that value on

the y axis. For the microscopy images, one or two peaks were typically on the brightness curve but more could occur. These peaks corresponded to the most common pixel brightness values in the image. The low assigned value was set to the left-bottom most point of the peaks and the high assigned value was set to the right-bottom most point of the peaks. This procedure changes the polymer phase in the image from a yellow-green to a green or yellow color and the asphalt phase in the image from a green to a black color. The overall effect of this imaging method is to give contrast to the two different phases.

The automatic exposure photos were used to examine the polymer morphology in the asphalt. The polymer structure in the asphalt was used to find a relationship with the DSR and forced ductility/ductility data. Hopefully this relationship will explain why some polymer modified asphalts perform better with aging than other polymer modified asphalts (*22*).

RESULTS AND DISCUSSION

Gel Permeation Chromatography

Figure 2-2 shows the GPC chromatograms of Koch PG 70-22 and Alon PG 70-22. Both binders are SBS modified binders. The polymer, in this case SBS, elutes first because the polymer has a higher molecular weight than the rest of the components in the asphalt binder. The data shown in the two following include both the specific viscosity detector, which is sensitive to the polymer concentration, and the refractive index (RI) detector, which is sensitive to the asphalt components. As measured by the peak heights, the Alon PG 70-22 initially has about 2.5 times the SBS as the Koch PG 70-22. At PAV*32 aging, the Alon PG 70-22 still has 2.5 times the SBS as the Koch PG 70-22 binder. However, it should be noted that GPC peak height is not necessarily a measure of the amount of polymer. Also playing significant roles are the peak width, shape and the location of the peak, all measures that relate to the polymer’s molecular size distribution.

Alon PG 70-22	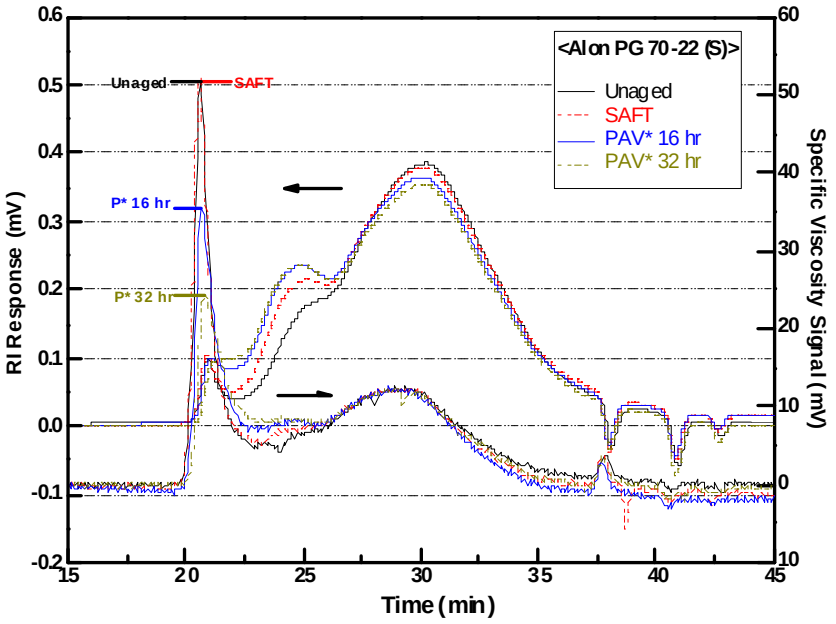
Koch PG 70-22	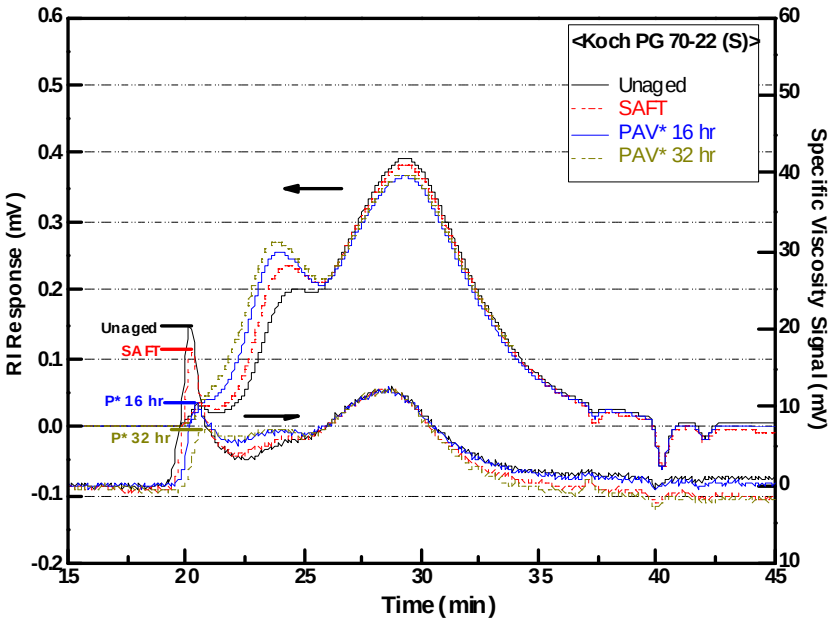

FIGURE 2-2 GPC of Koch 70-22 and Alon 70-22 (22)

Alon PG 76-22	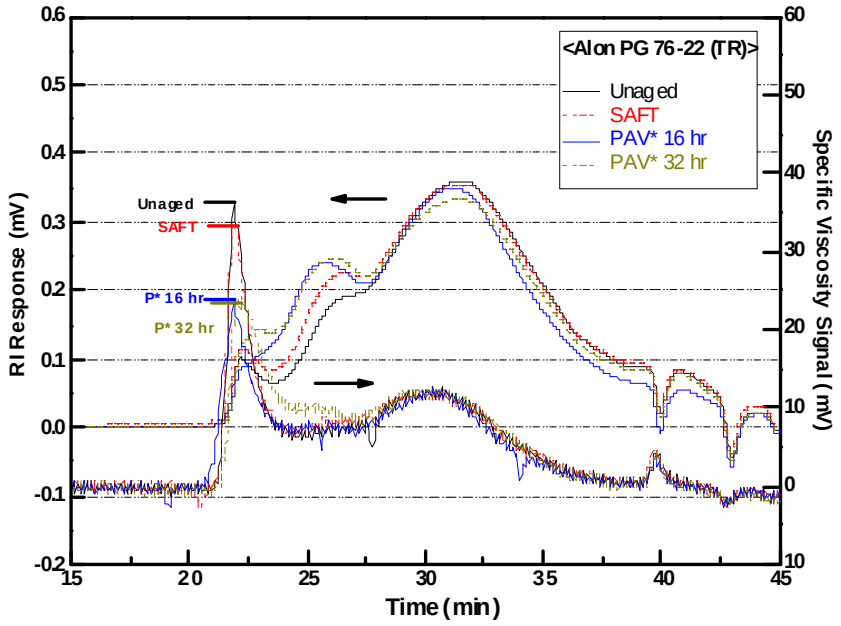
Koch PG 76-22	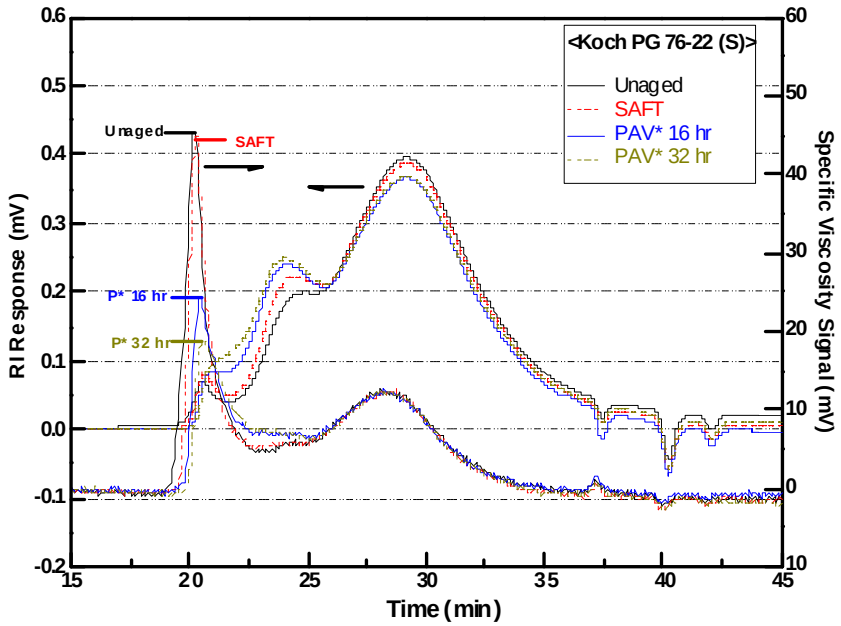

FIGURE 2-3 GPC of Koch 76-22 and Alon 76-22(22)

Figure 2-3 shows GPC results for the Koch PG 76-22 and Alon PG 76-22 materials. The Alon PG 76-22 clearly shows less polymer modifier than the Alon PG 70-

22. The Alon PG 76-22 is modified with both tire rubber (TR) and SBS. The chromatogram suggests that the higher grade PG 76-22 could be obtained by using less SBS than the PG 70-22 by adding TR. The TR is not seen in the chromatogram; most likely the rubber particles were removed by the 0.45 µm syringe filter. Unlike the Alon PG 76-22, The Koch PG 76-22 shows an increase in the polymer concentration compared to the Koch PG 70-22. This larger amount of polymer should be expected for a more heavily modified binder

Figures 2-4 and 2-5 focus on the RI detector chromatograms. The first peak is the polymer peak. The second and higher peak is the asphaltenes. The third and largest peak contains maltenes (both aromatics and saturates). The polymer elutes first because it has the largest molecular size and the maltenes elute last because they have the smallest (*24*).

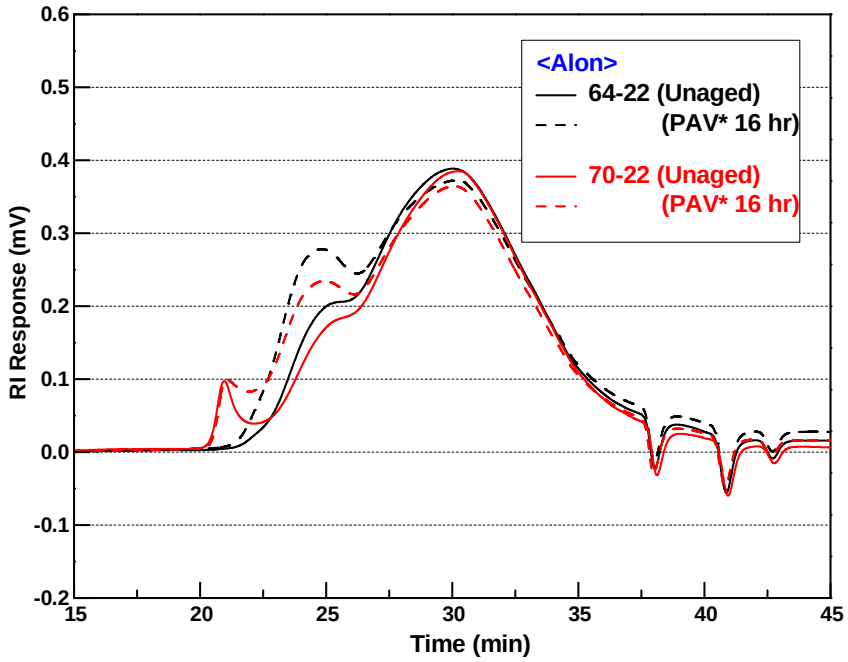

FIGURE 2-4 GPC Comparison Between Alon 64-22 and Alon 70-22 (22)

Figures 2-4 and 2-5 show the polymer has an interesting and profound effect on the asphalt base binders. The polymer appears to decrease the size of the asphaltene peaks of the two 64-22 base binders in Figures 2-4 and 2-5 perhaps due to polymer-asphalt interactions. These interactions may serve to disperse asphaltene associations thereby decreasing the asphaltene content from the base binder. The decrease in asphaltene content showed in Figures 2-4 and 2-5 could be very helpful in decreasing the stiffness of the binder as it ages, thereby enhancing the binder's ductility.

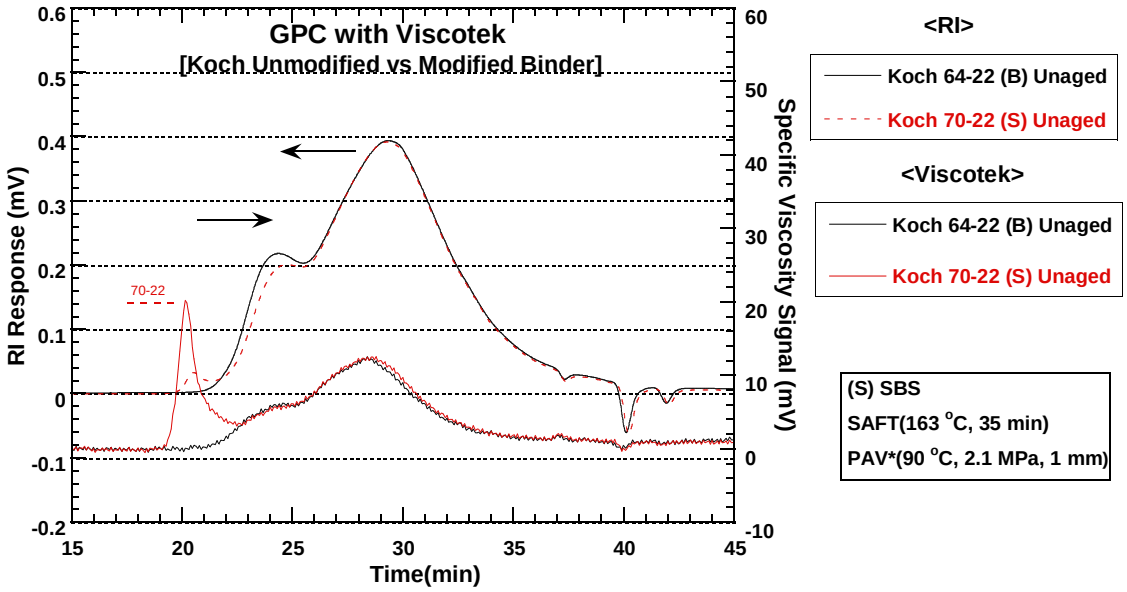

FIGURE 2-5 GPC Comparison Between Koch 64-22 and Koch 70-22 (22)

Dynamic Shear Rheometer

Figures 2-6 and 2-7 have 4 DSR maps with the different aging levels of the Koch and Alon binders. The DSR map shows log G' versus η'/G'. The dashed curves are points on the relationship discovered by Ruan et al. (*6*) that expand into a curve on the DSR map. The overall trend as asphalt binders in general age, and as these Koch and

Alon binders in particular age is for the binders to move from the lower right side of the map to the upper left side of the map. This movement corresponds to an increase in stiffness (G') and a decrease in the ductility (constant ductility lines) of the binder.

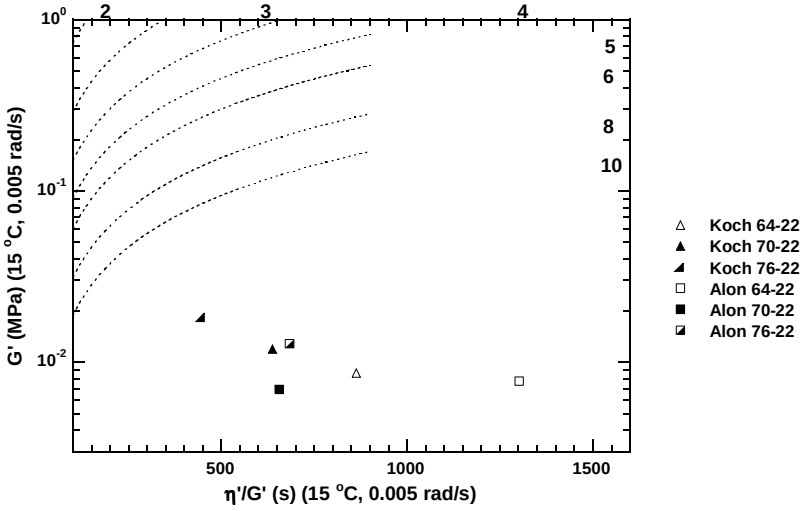

Unaged Binders

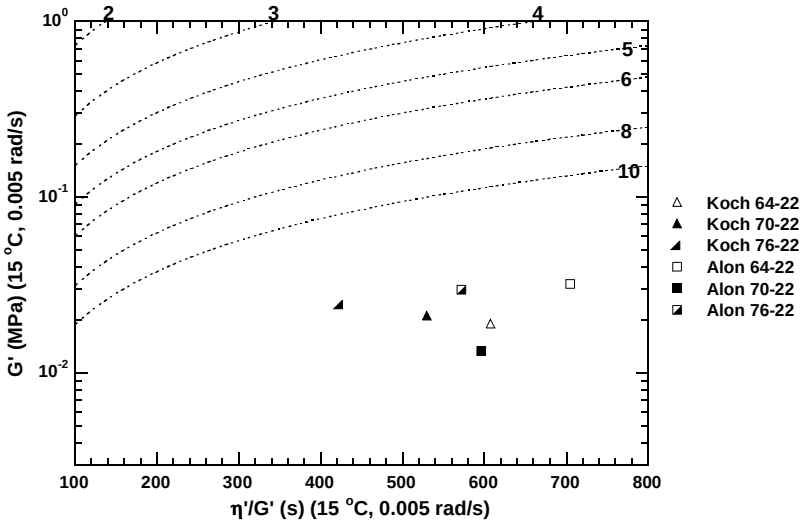

SAFT Aged Binders

FIGURE 2-6 Koch and Alon DSR Maps for Unaged and SAFT Aged Binders [data from (*22*)]

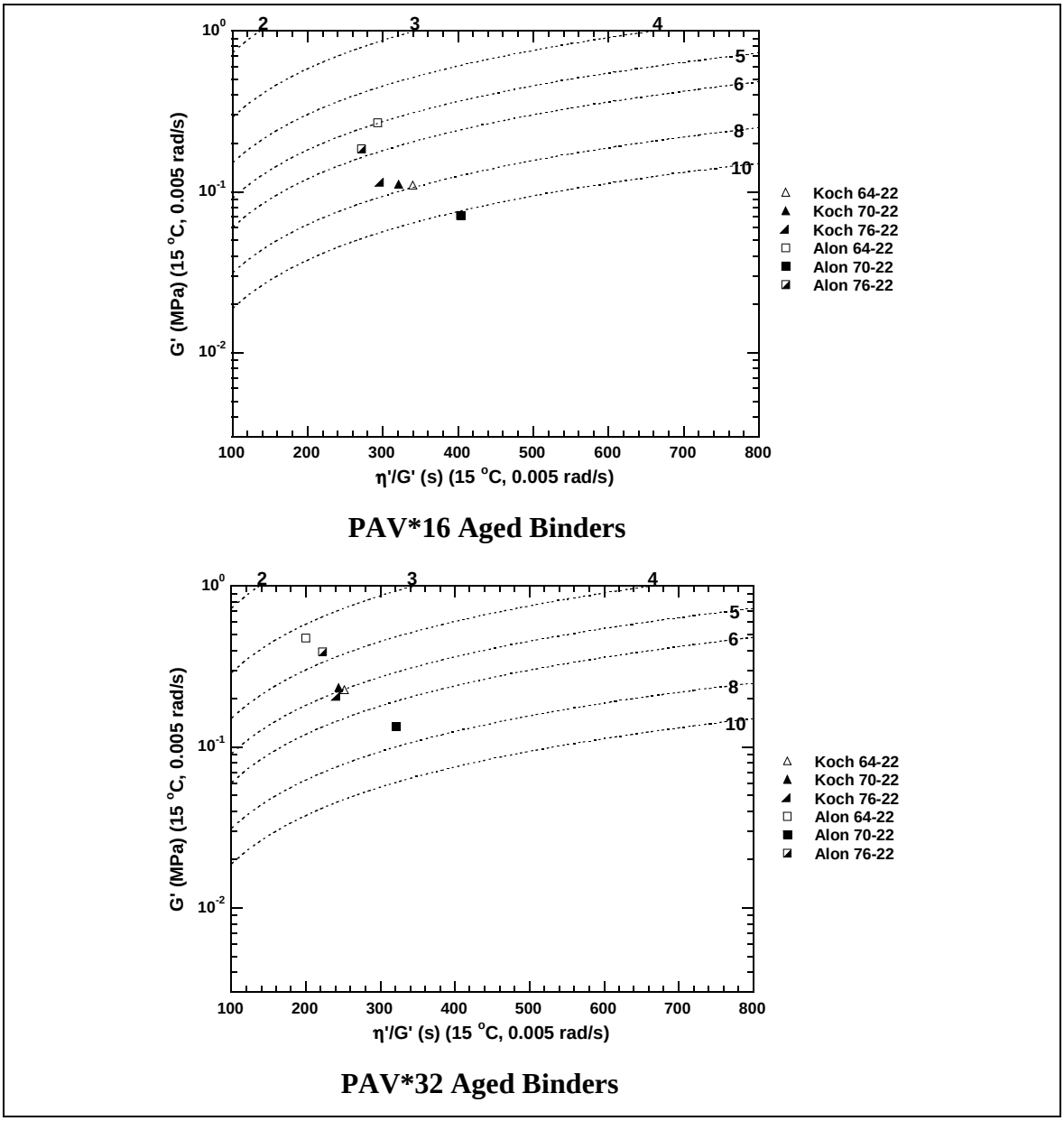

FIGURE 2-7 Koch and Alon DSR Maps for PAV*16 and PAV*32 Aged Binders [data from (*22*)]

DSR Function Ratio Divided by Polymer Concentration

Figure 2-8 is an amalgam of DSR and GPC data which may lead to insight on the ductility ratio which is explained later on in this chapter. To explain Figure 2-8, one must understand what the DSR function is and how you can use it. The DSR function is defined as G'/(η'/G'). The DSR Function comes from Equation 1-1 and is used to calculate the average unmodified binder ductility. By dividing the modified binder DSR function by the unmodified DSR function, the final value should correspond to a calculated average unmodified binder ductility ratio. This ratio when divided by the polymer peak height measured from the GPC gives an indication of the polymer's effectiveness at changing the DSR function in the binder. Figure 2-8 suggests that the Alon PG 70-22 is the most effective at modifying ductility for the amount of SBS modifier, as measured by the GPC. Further comment about modifier effectiveness will be made after the ductility ratio is discussed later in the chapter.

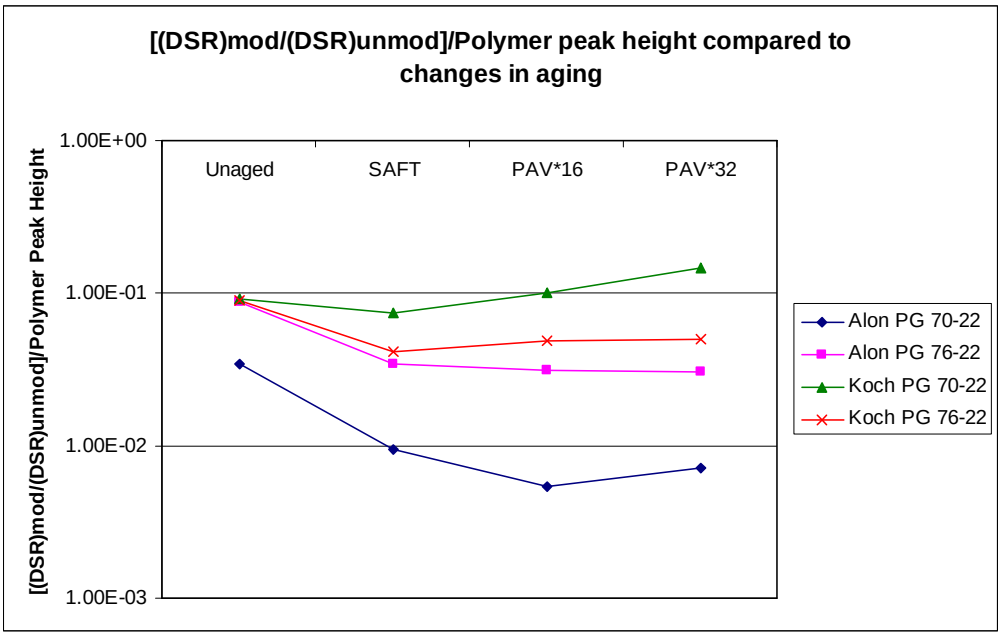

FIGURE 2-8 DSR Function Ratio Divided by Polymer Peak Height [data from (22)]

Microscopy

Introduction/Overview

The microscopy images below are used to analyze two different objectives. To examine the differences in the polymer morphology between binders and to evaluate the polymer morphology changes with oxidative aging. These objectives will hopefully lead to discovering the effects of polymer morphology on the initial problem and a possible system of polymer decay in the asphalt.

Fluorescence microscopy reveals a polymer phase and an asphalt phase. The asphalt phase is black in the image. The polymer phase is green if printed in color and shades of grey if viewed in black and white.

Images and Discussion

The Alon PG 70-22 Fluorescence Microscopy images are shown in Figure 2-9. The Unaged image has very distinct polymer phase bands. By SAFT aging, the polymer phase bands have begun to break down and the polymer has begun to spread across the image. In the PAV* 16 image the polymer has almost spread over the entire image and the initial bands have disappeared. With further aging, the polymer phase stops spreading and begins to disappear as displayed by the black bands in the PAV*32 image.

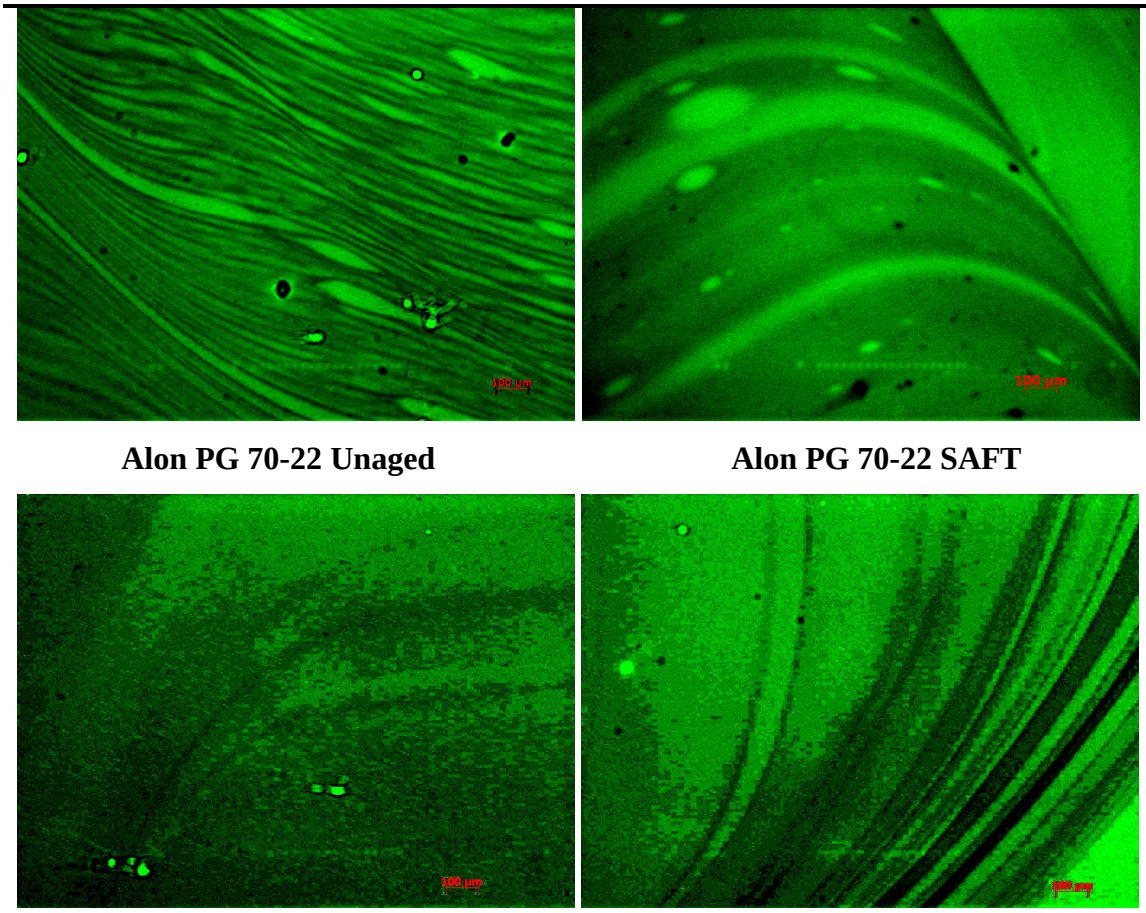

Alon PG 70-22 Unaged **Alon PG 70-22 SAFT**

Alon PG 70-22 PAV*16 **Alon PG 70-22 PAV*32**

FIGURE 2-9 Alon PG 70-22 Fluorescence Microscopy Images at 50x

The Koch PG 70-22 images in Figure 2-10 show similar trends to the Alon PG 70-22 images in Figure 2-9. The unaged Koch image looks very similar to the SAFT aged Alon PG 70-22 image. With SAFT aging the polymer spreads out and the polymer phase bands disappear making the SAFT image very similar to the Alon PG 70-22 PAV*16 image. By PAV*16 aging the polymer has spread almost evenly over the entire image. The PAV*32 image has some black area but is not like the bands shown in Figure 2-9.

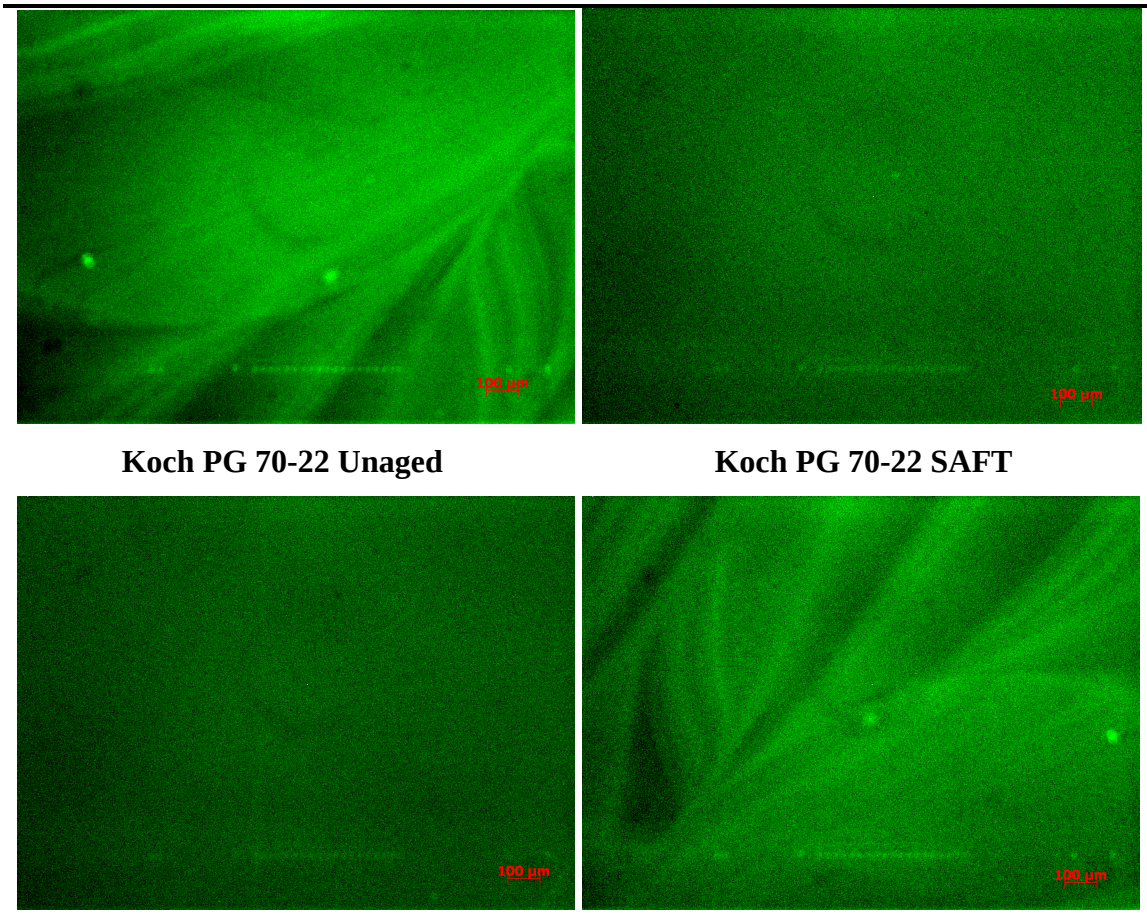

Koch PG 70-22 Unaged **Koch PG 70-22 SAFT**

Koch PG 70-22 PAV*16 **Koch PG 70-22 PAV*32**

FIGURE 2-10 Koch PG 70-22 Fluorescence Microscopy Images at 50x

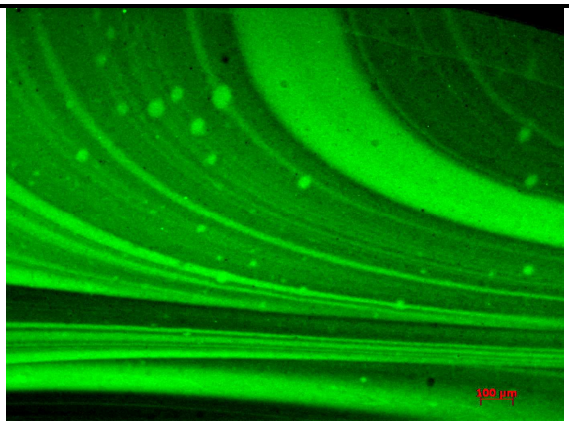

Alon PG 76-22 Unaged

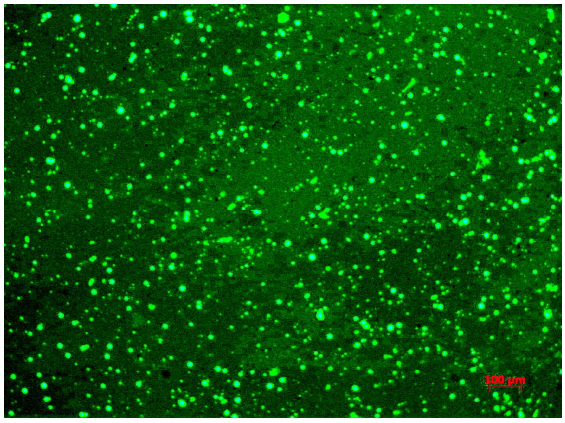

Alon PG 76-22 PAV*16

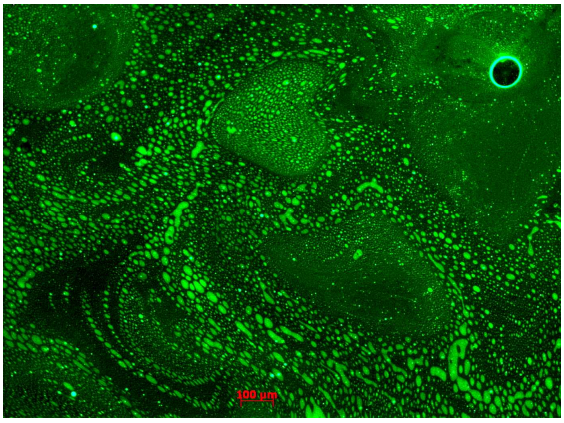

Alon PG 76-22 PAV*32

FIGURE 2-11 Alon PG 76-22 Fluorescence Microscopy Images at 50x

Because Alon PG 76-22 has both tire rubber (TR) and SBS, Figure 2-11 cannot really be compared very easily to the other binders' fluorescence microscopy images. Therefore, for Figure 2-11, just the Alon PG 76-22 binders will be discussed. The polymer phase bands in the unaged binder, which are similar to those in the Alon PG 70-22 unaged image, are believed to be the SBS. The particles which are in an array of sizes in the unaged image are believed to be the TR. All of these particles are bigger than the pore size of the GPC filter which means the TR would not show up in the GPC data. The GPC data in Figures 2-2 and 2-3 show that the Alon PG 76-22 has less polymer peak

height than the Alon PG 70-22. The microscopy images offer a reasonable explanation as to why the decrease occurs.

The size and shape of the polymer change as the binder ages to PAV* aging levels. The SBS for the PAV* images is now a haze rather than bands. The TR, which was originally large particles are now smaller particles in the PAV* images. Some of the TR particles in the PAV*32 image are forming green areas around them. These green areas may be a sign the TR is breaking down. The GPC results in Figures 2-2 and 2-3 may offer confirmation of the TR breaking down in the PAV*32 image. The polymer peak height in the GPC curves decreases with aging for all of the asphalt binders shown except for the Alon PG 76-22 PAV* 32 binder. The Alon PG 76-22 PAV*32 binder has a higher polymer peak height than the Alon PG 76-22 PAV*16 binder. One possible explanation could be the green areas around the particles can now travel through the 0.45 µm filter and be measured by the GPC. These green TR areas would replace the broken down SBS, therefore, the polymer peak height measured by the GPC would change very little from the PAV* 16 to the PAV*32 aging levels. The microscopy images combined with the GPC give a very interesting look into how the TR behaves in the asphalt binder.

The microscopy images from the Koch PG 76-22 binder (Figure 2-12) are very similar to the images in Figure 2-10 from the Koch PG 70-22 binder. The unaged Koch PG 76-22 image is very similar to the Koch PG 70-22 image but the Koch PG 76-22 image shows more definition to the phase boundaries most likely because the PG 76-22 has a higher polymer peak height than the PG 70-22 binder. Interestingly, the Koch PG 76-22 SAFT image looks simply like a brighter version of the Koch PG 70-22 SAFT image. This result suggests that increasing the polymer content in a binder may have little effect on the polymer morphology with aging.

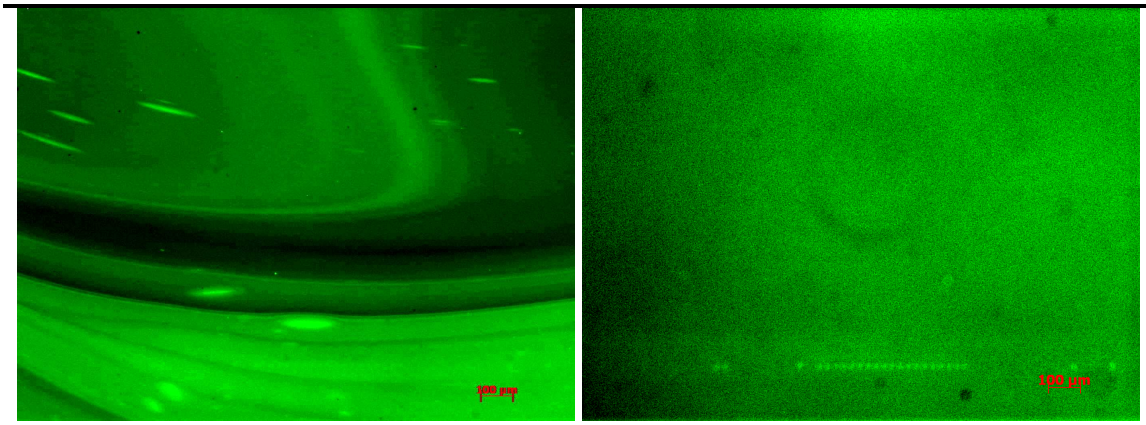

Koch PG 76-22 Unaged **Koch PG 76-22 SAFT**

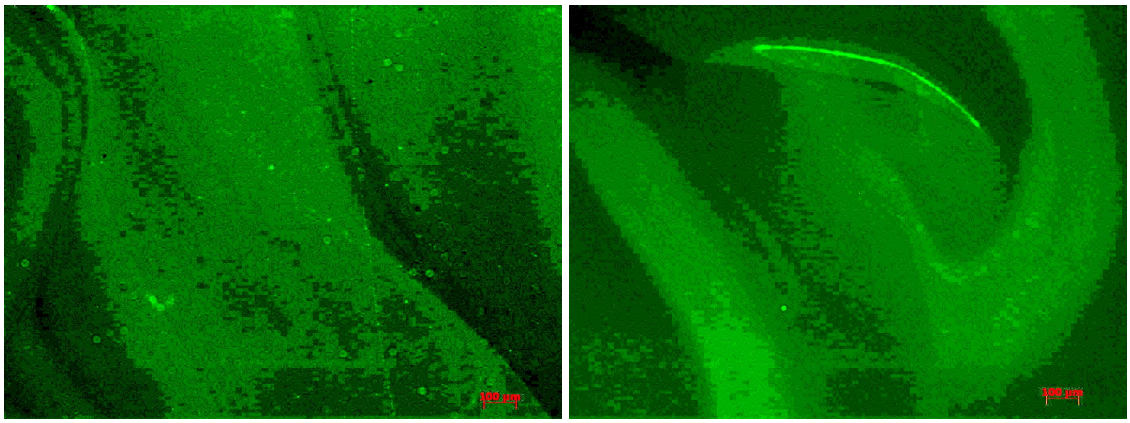

Koch PG 76-22 PAV*16 **Koch PG 76-22 PAV*32**

FIGURE 2-12 Koch 76-22 Fluorescence Microscopy Images at 50x

The images shown in Figures 2-9 through 2-12 show a general trend for the SBS. The SBS phase in the beginning tends to start out in polymer phase bands in the asphalt binder. As the asphalt ages the SBS phase bands break down and the SBS phase spreads across the image. At some point in the aging process, the SBS phase stops spreading out, but the SBS continues to break down leaving black spaces (asphalt phase) in the image. These black spaces are noticeable in the PAV*32 images.

SBS Properties

Before discussing a proposed mechanism, the properties of SBS need to be explained. SBS is a thermoplastic block polymer made with Polystyrene and Butadiene Blocks. The polystyrene blocks aggregate and form three dimensional elastic networks made from the polybutadiene blocks. This aggregation process occurs because the polystyrene blocks are able to form physical cross-links (*25*). Unfortunately, fluorescence microscopy does not show the polybutadiene or polystyrene phases but can estimate the degree of cross-linking by examining how close together the SBS concentrated phases are.

In the microscopy images shown in Figures 2-9 through 2-12, there are two types of structuring in the SBS phase of the images. The two types are high structure and low structure. High structure refers to the SBS having a higher chance of physical cross-linking in the SBS phase. High structure tends to exist at Unaged and SAFT aging levels. Low structure refers to the SBS having a lower chance of physical cross-linking in the SBS phase. Low Structure can exist at any asphalt aging level, but low structure is seen in great quantity at PAV* 16 and PAV*32 aging levels. A visual explanation of these structures can be found in Appendix A.

SBS breaks down by itself and in the asphalt through a series of thermo-oxidative radical reactions. Cortizo et al. (*20*) noticed the SBS polymer reacts differently in the polymeric form than in the asphalt. Pure SBS reacts through chain scission or chain transfer. These reactions can occur in both the butadiene and styrene blocks. The pure SBS breaks down into lower and higher molecular weight fractions as well as an insoluble (THF solvent) cross-linked gel which is the main degradation product of the pure SBS. When the SBS is added to the asphalt binder, the SBS breaks down slightly differently. The reaction mainly consists of chain scission which breaks the SBS into lower molecular weight polymer. Cortizo et al. also believes the SBS can radical addition to some of the components in the asphalt (*20*). The SBS decay reactions in the asphalt should lead to a breakdown of the original polymer network.

Proposed Mechanism

Combining the information on SBS chemical breakdown and physical cross-linking with the general trends from Figures 2-9 through 2-12, we can come up with a hypothetical proposed mechanism for SBS breakdown in asphalt binder. A graphical version of the hypothetical proposed mechanism is shown in Figure 2-13. The mechanism shows, as the asphalt ages, the high structure SBS breaks down into low structure SBS which spreads across the image filling up the black spaces. Once most of the black space in the image is filled, the low structure SBS breaks down with continued aging into the low concentration SBS phase (Asphalt phase). Eventually, although not shown in any of the images, the binder will be all low concentration SBS phase (Asphalt phase).

This mechanism can also be used to explain why the Alon binders have a higher ductility enhancement then the Koch binders at PAV* aging condition. Examining the microscopy images, the Alon binders should have a higher amount of physical cross-linking than the Koch binders initially. Because Alon binders are believed to have more physical cross-linking initially than Koch binders, Alon binders should still have more physical cross-linking even at PAV* aging levels. More physical cross-linking should correspond with a more elastic material. A more elastic material should stretch more than a less elastic material. Therefore, Alon binders, believed to be the more elastic material, have better ductility enhancement.

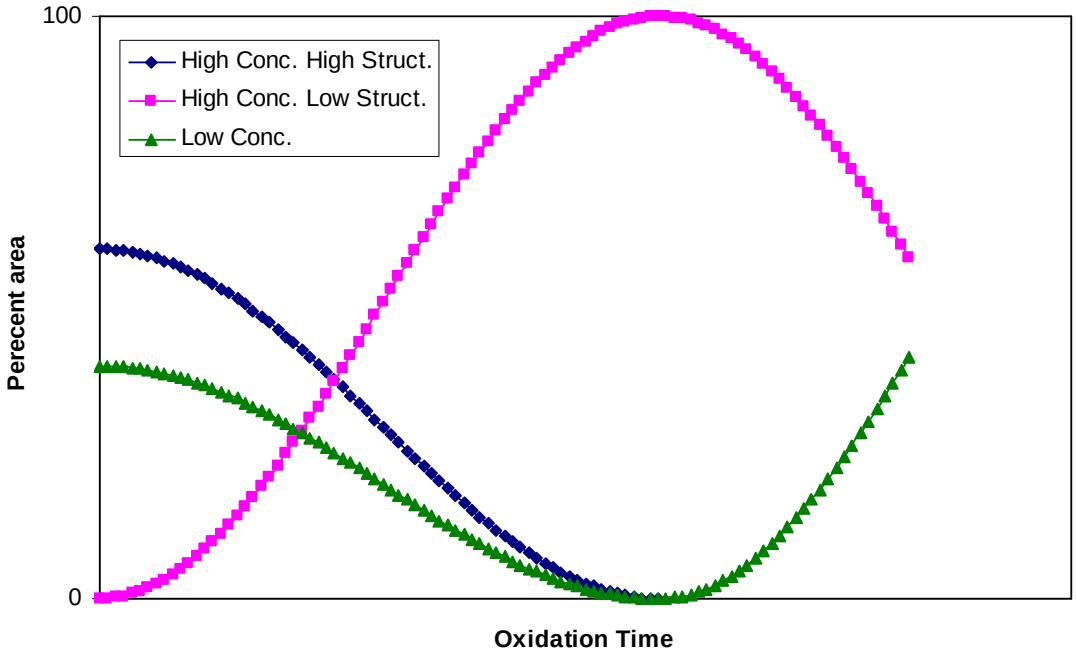

FIGURE 2-13 Proposed Hypothetical SBS Breakdown Mechanism in Asphalt Binder

Force Ductility

Examining Figure 2-14, the PAV* aged polymer modified binders do not show a polymer-asphalt modulus but still have an asphalt modulus. These two moduli are graphically depicted in Figure 1-1. The asphalt-polymer modulus is thought to arise from asphaltene and polymer interactions and uncoiling of polymer chains (*21*). A lack of an asphalt –polymer modulus for the PAV* aged binders would then mean the polymer at this temperature is not able to interact with the asphaltenes. Ironically, in a paper by Woo et al., polymer modified binders showed an asphalt-polymer modulus when the binders were heated to 10 °C. These binders also showed no asphalt-polymer modulus at the lower temperature, 4 °C, of the force ductility test (*26*).

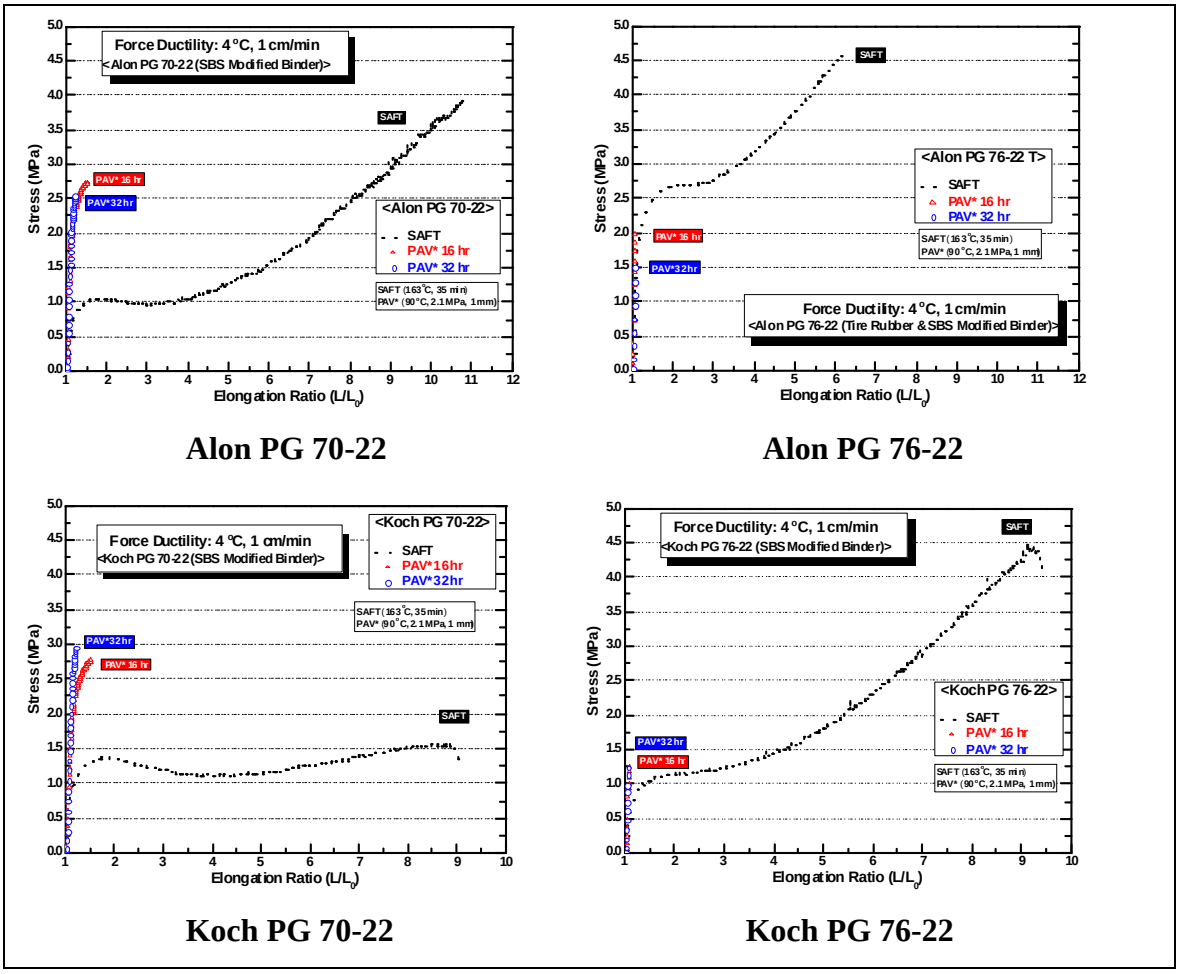

FIGURE 2-14 Force Ductility Data for Alon and Koch Polymer Modified Binders

If we combine the above analysis on force ductility with the microscopy analysis, some very interesting ideas about the loss of the asphalt-polymer modulus can be created. The microscopy data show at the PAV* aging level, the binder mainly consists of low structure SBS. So the binder definitely has SBS still inside but the force ductility test at 4 °C doesn't show any of the polymer's increased elongation effects. When the temperature of the force ductility test is increased those increased elongation effects return. The best explanation for these force ductility results is the low structure polymer can not handle the increased loading rate of the 4 °C test and so the increased

elongation/asphalt polymer modulus are never seen. But when the temperature of the force ductility test is increased, the loading rate decreases, and therefore, the increased elongation/asphalt polymer modulus appears.

Ductility

The ductility of the Koch and Alon binders are shown below in Figure 2-15. Figure 2-15 shows the polymer modified binders at PAV* aging levels show increased ductility from the polymer's effects. The explanation in the previous paragraph should be a good explanation of why the ductility, which is at a higher temperature than the force ductility test, shows the enhanced elongation of the polymer but the force ductility test does not. Also of note is that the unmodified Alon PAV* aged binders have very low ductility around 1 cm. But the modified Alon PAV* aged binders have their ductility between 5 to 10 cm. This difference between the modified and unmodified binder ductility will be discussed in the next sub section on ductility ratio.

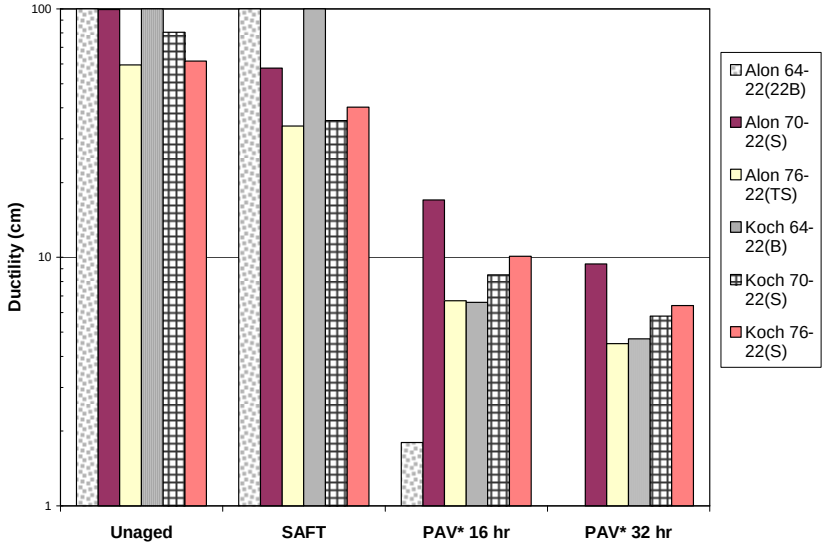

FIGURE 2-15 Ductility Bar Graph for Koch and Alon Binders

Ductility Ratio

The ductility ratios shown in Table 2-2 when examined with the microscopy data show that the microscopic structure of the polymer has a very large effect on the ductility improvement at PAV* aging. Table 2-2 shows the Alon binders have a higher ductility ratio than the Koch binders. The microscopy data show the Alon binders have higher polymer structure concentration at unaged levels than the Koch binders. The ductility ratios match the order of the high structure polymer concentration in the unaged binders, except the Alon PG 76-22. The Alon PG 76-22 is below the Alon PG 70-22 in ductility ratio yet has a higher concentration of high structure polymer. This exception is most likely caused by the added TR.

TABLE 2-2 Ductility Ratio of Koch and Alon Polymer Modified Binders

	Ductility Ratio (Modified binder ductility/unmodified binder ductility)	
	PAV*16	PAV*32
Alon70-22(S)	9.4	9.4
Alon76-22(TS)	3.7	4.5
Koch70-22(S)	1.3	1.2
Koch76-22(S)	1.5	1.4

Examining the Effects of Polymer Concentration on Ductility Ratio

Figure 2-16 and Figure 2-17 examine the effectiveness of the polymer for enhancing ductility. Figure 2-16 shows at unaged and SAFT aging levels the polymer has almost no affect on improving the ductility. But at PAV* aging levels, the polymer becomes more effective in improving the ductility. Figure 2-16 also shows different binders have different ductility enhancements from adding polymer. Are these enhancements related to adding more polymer or related to the polymer morphology? Figure 2-17 answers this question and shows the ductility enhancement from the polymer does not correlate well to the polymer peak height. Figure 2-17 also suggests another factor may be involved. The most likely factor is polymer morphology.

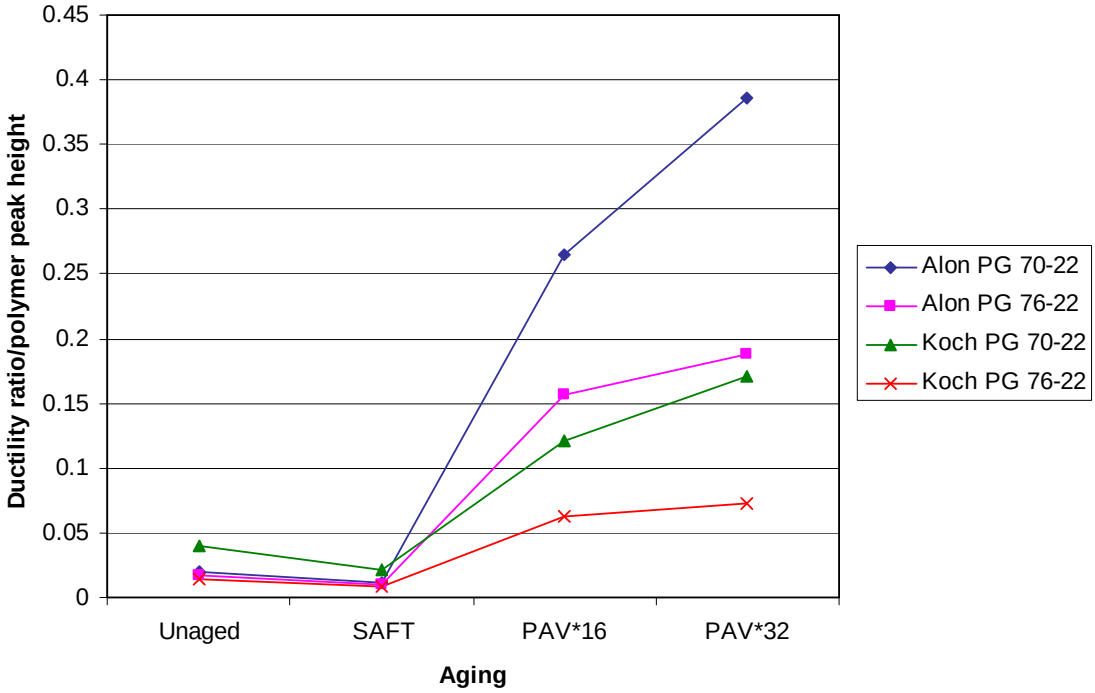

FIGURE 2-16 Ductility Ratio Divided by Polymer Peak Height Versus Aging Levels

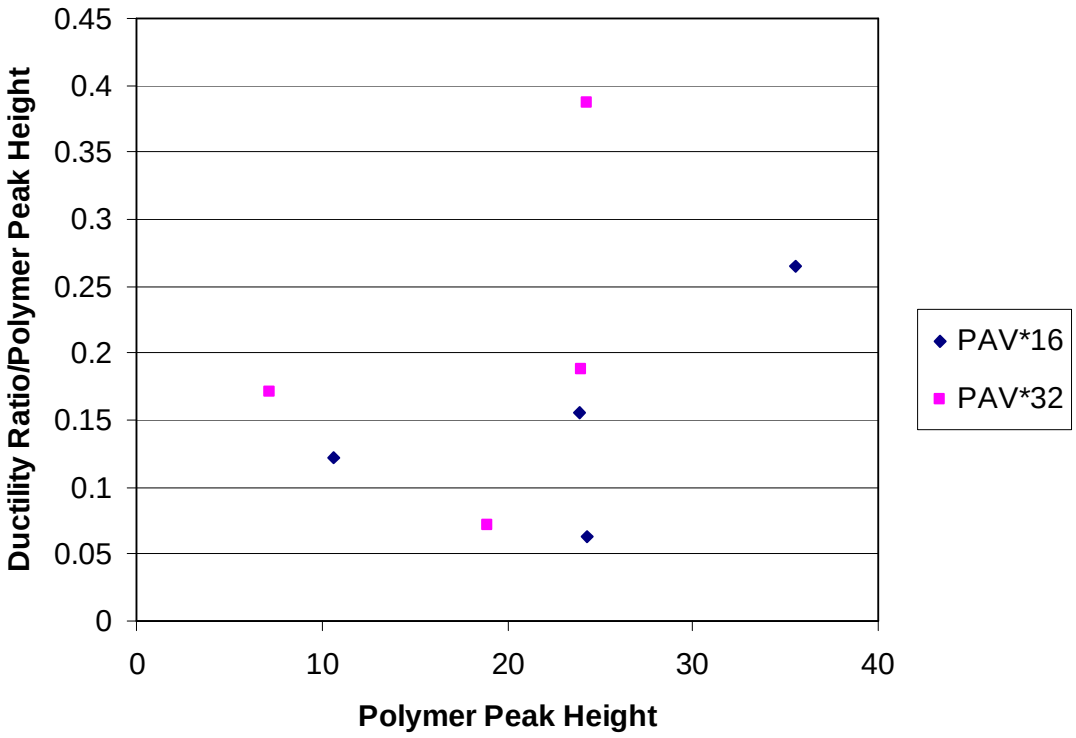

FIGURE 2-17 Ductility Ratio Divided by Polymer Peak Height Versus Polymer Peak Height

DSR Function Ratio Divided by Polymer Concentration Compared with Ductility Ratio

The DSR function ratio divided by the polymer concentration was examined earlier as to whether the relationship had any correspondence with ductility ratio. To answer this question, the DSR function ratio divided by the polymer concentration and the ductility ratio were graphed on Figure 2-18. Figure 2-18 shows Alon PG 70-22 has the highest ductility ratio and the lowest DSR ratio/polymer peak height. Koch 70-22 has the lowest ductility ratio and the highest DSR ratio/polymer peak height. Figure 2-18 clearly shows a relationship between the ductility ratio and the DSR function ratio divided by the polymer concentration. This relationship shows as the DSR ratio/polymer concentration decreases the ductility ratio increases.

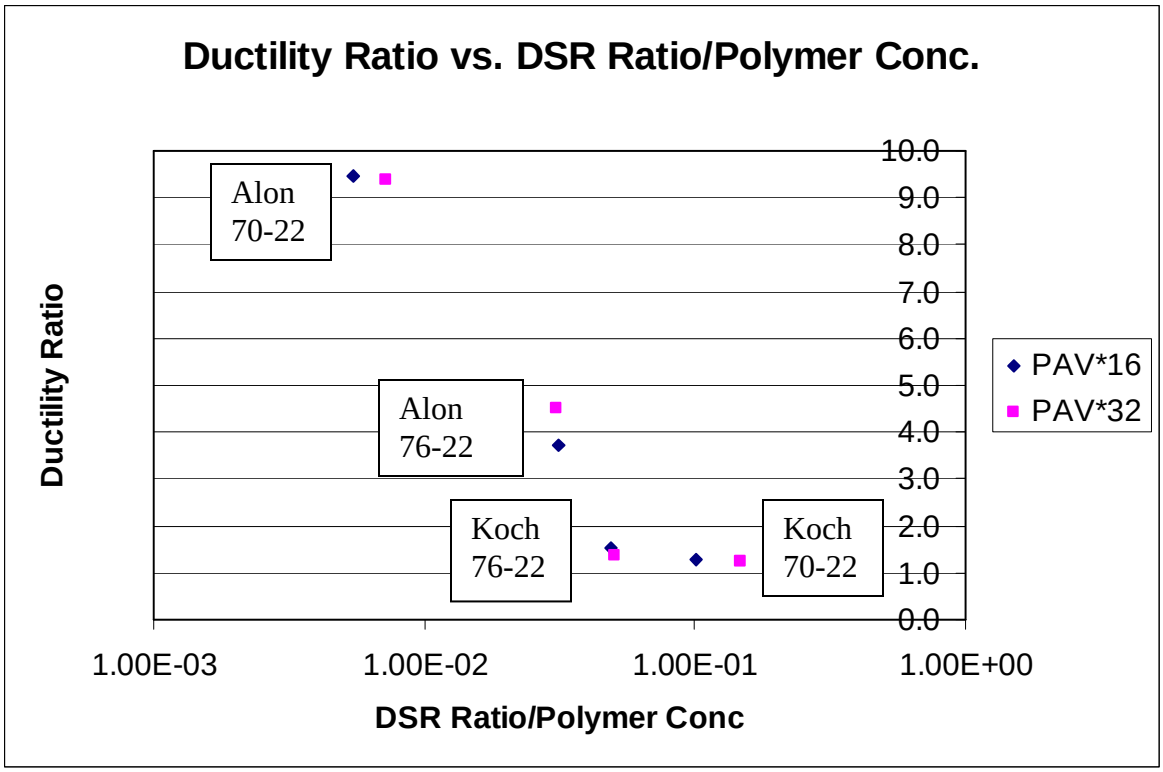

FIGURE 2-18 Ductility Ratio Versus DSR Ratio/Polymer Concentration for Alon and Koch Polymer Modified binders at PAV* aging Conditions

CONCLUSIONS

The Microscopy data give a clear picture as to why the Alon modified binders have better ductility enhancement than the Koch modified binders. Microscopy also was helpful in coming up with an explanation of how the SBS breaks down in the asphalt binder. Microscopy was also used to explain why the effects of the polymer could not be seen at the temperatures of the force ductility test but could be seen at the temperature of the ductility test. Also, the DSR Ratio divided by the polymer concentration was found to correlate with the ductility ratio and gave another reason to explain why the Alon modified binders had higher ductility enhancement than the Koch modified binders.

CHAPTER III
USING BINDER RHEOLOGY TO DECREASE RAVELING OF MIXTURE DESIGNS

INTRODUCTION

The purpose of this chapter is to report a relationship between the binder's DSR function and the mixture's Cantabro loss. Cantabro Loss data from the TxDOT project 0-5262, Optimizing the Design of Permeable Friction Courses (PFC), were used. The goals of this project were: to create a design guideline for Permeable Friction Course (PFC) in Texas, test the PFC currently on the road and relate binder properties to PFC durability. The binders tested are the following: US-281-AR, US-288-AR, IH-35-PG-76-22, IH-30-PG-76-22, IH-20-PG-76-22, US-59-PG-76-22, IH-20-PG-76-22TR. The only mixture for which data is not discussed is IH-20-PG-76-22TR because no Cantabro Loss experiments were done on this mixture. Hopefully relating the DSR function data from the binder with the mixture's Cantabro loss will lead to a new relationship. All mixture measurements were made by researchers in the Zachry Department of Civil Engineering at Texas A&M University.

Most of the extracted mixture data have been placed in Appendix B because the rheology in this chapter deals with binder data not extracted binder. An explanation of why just the binder and not the extracted binder data were used is given later in this chapter. Also the viscosity and phase angle curves for some of the binders can be found in Appendix B as well.

METHODOLOGY

The research experiments were divided into two groups based on whether the research was binder based or mixture based. The binder based research was conducted within the chemical engineering research group. The mixture based research was done by

the civil engineering research group and includes mixture design and Cantabro testing. The rest of this section explains the methods and steps used for binder testing and aging.

Four levels of aging were used in these two projects. These four levels of aging were Unaged, SAFT, PAV*16 and PAV*32. Seventy grams of the unaged, SAFT, PAV*16 and PAV*32 asphalt were needed for further testing. To acquire the SAFT, PAV*16 and PAV* 32 asphalt, two 250 g batches of asphalt were SAFT aged. The SAFT aging procedure was to stir 250 g of asphalt binder in an air flow vessel at 325° F (163° C) for 35 minutes while air is being blown into the asphalt. The stirring was done at 700 RPM and the air flow rate was 2000 mL/min. After SAFT, 170 g of SAFT aged binder were PAV* aged. To do the PAV* test 17g of asphalt was melted into a PAV pan to form a 1 mm thick layer. The pressure and temperature of the PAV* test were 2.2 MPa and 90° C. The PAV*16 procedure needed 10 pans and lasted 16 hours. After the PAV*16 aging was finished, five of the PAV*16 pans continued to be aged for another sixteen hours using the PAV* aging conditions. These two PAV* aging steps produced 75 g of PAV*16 and PAV*32 asphalt binder. These four levels of aging allowed lab testing on binders aged up to the equivalent of 6 years in the pavement (*27*).

Ductility and force ductility were used to assess the ability of the binder to withstand elongation. The force ductility test was conducted at 4 °C with an extension rate of 1 cm/min. The initial sample had a gauge length of 3 cm and a uniform cross section in the middle of 1 cm by 0.5 cm. The force ductility test measures force as a function of extension ratio. The ductility test was conducted at 15 °C with an extension ratio of 1 cm/min. The initial sample had a gauge length of 3 cm and a tapered cross section. The ductility measures the maximum extension of the binder. Although ductility and force ductility do not give as much information or the same type of information as the DSR, Ductility and force ductility still measure the effect of binder stiffness on the asphalt's ability to elongate without cracking failure (*27*).

DSR measurements were the primary rheological test method and involved three testing methods. The DSR test was done using a Carri-Med CSL500 dynamic shear rheometer. Enough sample of asphalt was applied to the test surface to fill the gap

between the surface and the plate after the 2.5 cm plate squeezed the sample. The gap size used was 500 µm for the SBS and TR binders and 1500 µm for the AR binders. The excess sample then was scraped away. The three testing methods were carried out at 44.7, 60 and 80 °C. The first test was at 60 °C and used frequencies from 0.1 to 100 rad/s. The second test decreased the temperature from 60 °C to 44.7 °C and was conducted at 10 rad/s. For the third test the temperature was increased to 80 °C and again used frequencies from 0.1 to 100 rad/s. A master curve was created from the 60 and 80 °C DSR test using time-temperature superposition. The base temperature for the master curve was 60 °C. The 44.7 °C data gives G' and G", with the latter used to calculate η' (*27*). These G' and η' values correlate to the ductility from Equation 1-1. These three testing methods gave a very broad view of the rheology of the asphalt binder being tested.

The extraction and recovery procedures are explained in a paper by Burr et al. (*28*). The extraction procedure dissolved the asphalt mixture in an ethanol toluene solution (ethanol 15% by volume). The solution then was filtered and centrifuged to remove any dust and small particles from the mixture. The binder was recovered by heating the solution in a rotovap under vacuum conditions to evaporate the solvent. Initially the temperature of the rotovap was set to 212 °F but then was changed to 345 °F when none of the ethanol toluene solution is seen condensing in the rotovap. The extraction and recovery of the mixtures in this chapter and Apendix B follow these directions.

Some of the extraction and recovery was done on asphalt rubber binder; the procedure in this case was modified slightly. Twenty grams of AR binder were added to a beaker and then the same procedure of dissolving, filtering and recovering the binder was followed. The AR binder or mixture when extracted lost the rubber particles in the extraction process and altered the extracted binder into an unmodified binder. This process is explained later in the chapter.

BINDER RHEOLOGY

Asphalt Rubber Binders

Asphalt rubber (AR) is an asphalt binder with 15 to 21 percent crumb rubber produced by the MacDonald process, also known as the wet process (29). In addition to the wet process, a dry process also exists. The dry process adds the rubber directly to the aggregate rather than to the binder. Arizona began using asphalt rubber in 1964. Today, Arizona still uses AR. Arizona has used AR for seal coats, stress absorbing membranes (SAM), stress absorbing membrane interlayers (SAMI), open-graded mixes, and gap-graded mixes. Reported benefits of the AR wet process are improved reflection cracking, improved durability, decreased noise, and improved environmental impact, having reused 4 million tires since 1988 (*29*).

The laboratory observations of the AR binder have experimental difficulties which make accurate testing of the binder difficult. Many of these testing difficulties come from the large size rubber particles in the AR binder. Because of the large size rubber particles, the DSR test needed to be modified. This modification to the DSR test is explained in this section. This section also discusses the test results of the AR and how the results compare to a typical SBS or unmodified binder.

DSR Map

Figure 3-1 is the DSR map of the US-281-AR and US-288-AR binders but also includes extracted and recovered US-281-AR binder as well. The AR binders in Figure 3-1 behave differently than a typical binder. A typical binder (modified or unmodified) usually starts at the bottom right and moves towards the top left with aging. This movement corresponds with an increase in stiffness and a loss in the ductility of the binder. Unlike a typical binder, the AR binder begins on the far left of the map and moves towards the left upper corner with aging. Since the AR's initial position is on the

far left side, the ductility of the unaged AR binder should in theory be significantly less than a typical unaged binder. The Recovered binders, on the other hand, do not follow the trend of the AR binders in the figure; instead, they follow the trend of a typical binder. The Recovered binder's trend is indicative of the loss of rubber particles during the extraction process.

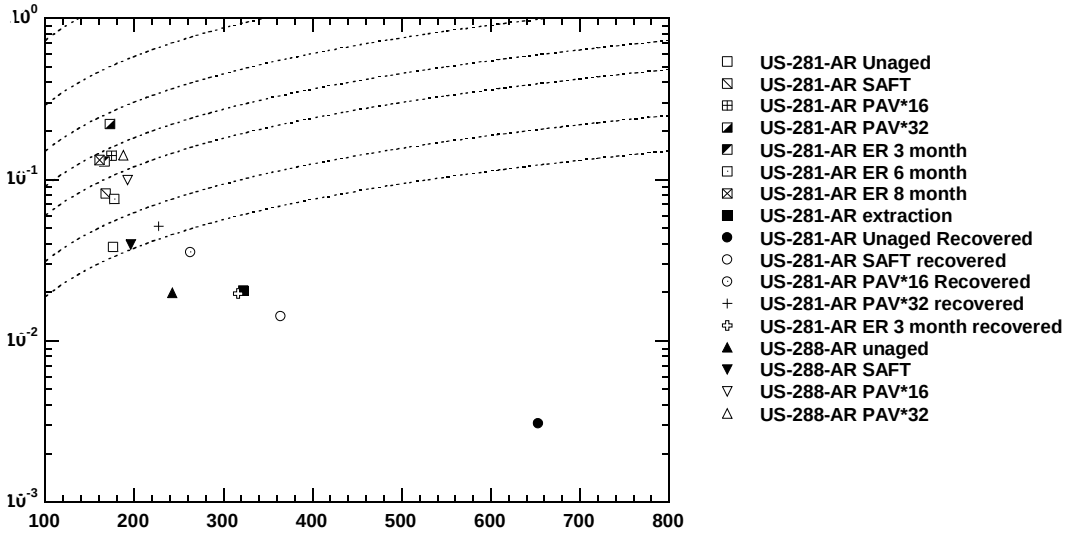

FIGURE 3-1 DSR Map for US-281-AR and US-288-AR Binders

Phase Angle Measurements to Explain Dynamic Shear Rheometer Gap Size

The AR consists of small particles of Rubber, some of which are big enough that when the two plates of the DSR come together the DSR measures the rubber particles and not the AR. Because of this phenomenon, testing on the AR binder needs to be done to get an estimate of the appropriate gap size that minimizes the rubber particle interactions and maximizes the Asphalt rubber interactions between the two plates. To determine this appropriate gap size, the AR binder's phase angle curve is measured at

different gap sizes. When the phase angle curves stabilize the correct gap has been found. (*30*).

At 1000 µm, Figure 3-2 shows the rubber particles in the binder are being pinched by the plates, therefore the properties of the rubber are measured and not the binder. The pinching of these particles is clear because the material properties are almost entirely elastic instead of being viscoelastic like a typical polymer modified asphalt binder. As the gap is increased to 1250 µm and higher, the binder behavior becomes more viscoelastic. At 1500 µm, Figure 3-2 shows the binder phase angle properties stabilize; therefore, the rubber particles are not being pinched by the two plates and the DSR should give correct rheology measurements.

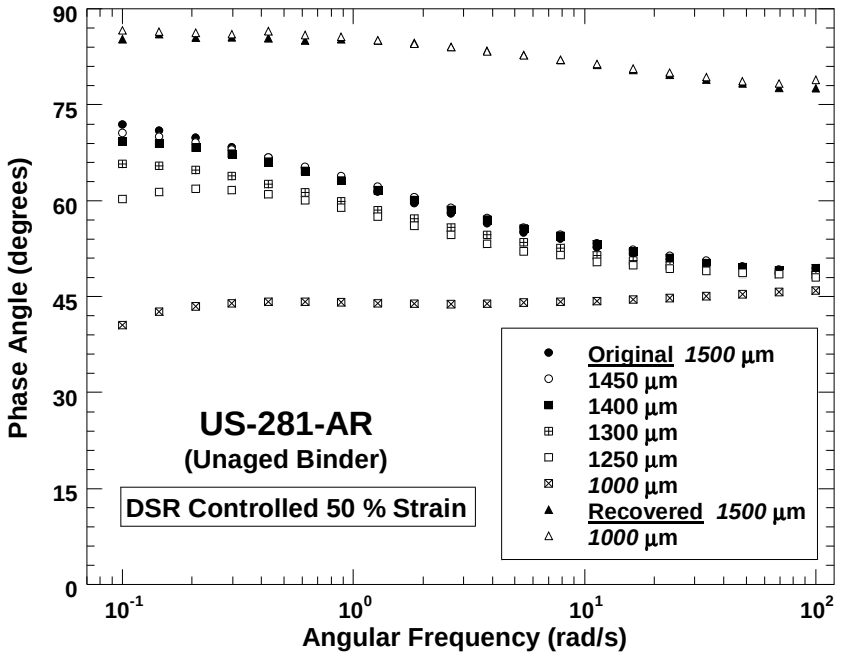

FIGURE 3-2 Phase Angle for Original and Recovered US-281-AR Binder

Figure 3-2 shows the recovered binder has a much higher phase angle than the AR binder. The recovered binder is the AR Binder which has been placed through the

extraction process. The extraction process will not allow the rubber particles to stay in the binder due to a 0.45 µm filter being used. Because of the lost rubber particles, the recovered binder's phase angle increases. The increased phase angle corresponds with a loss of elasticity with the material. The lost rubber particles explain why the recovered binder has a very different phase angle curve from the other binders in Figure 3-2.

Ductility Versus DSR Function

Figure 3-3 shows the ductility versus DSR Function for the asphalt rubber binders. The binders shown have less ductility than unmodified binders because they are below the unmodified ductility line described by Ruan et al. (*6*). This lower ductility may lead to an increased probability of mixture durability issues. A higher chance of durability issues will most likely lower the life of the PFC layer as well. In conclusion, the asphalt rubber has lower ductility than a typical unmodified binder and the mixture may have durability issues earlier than suspected because of the decreased ductility.

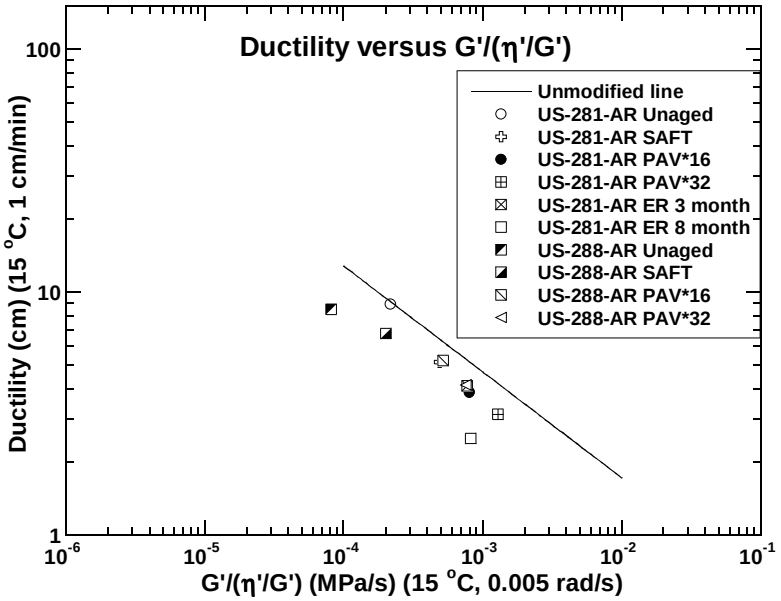

FIGURE 3-3 Ductility Versus DSR Function for Asphalt Rubber Binders

Ductility

Figure 3-4 displays both PAV*32 and PAV*16 binders as having their ductility below 5 cm. A ductility of between 3 and 5 cm is a benchmark for possible pavement durability issues (*31*). Not only do the binders have low ductility at PAV* aging but they also have low ductility at unaged and SAFT aged levels. The ductility for the SAFT and Unaged binders is between 5 cm and 9 cm. This ductility is extremely low for these two aging levels especially when comparing Figure 3-4 with the other ductility data (Figures 3-8 and 2-15). The ductility for Unaged and SAFT aged binders on these other graphs is between 30 cm and 100 cm. The AR binders may have durability issues with aging because the AR binders initially tend to have lower ductility then a typical binder and low ductility (below 5 cm) has been shown to increase the likelihood of pavement durability issues (*31*). But in the case of asphalt rubber, ductility may or may not show a relationship with mixture durability.

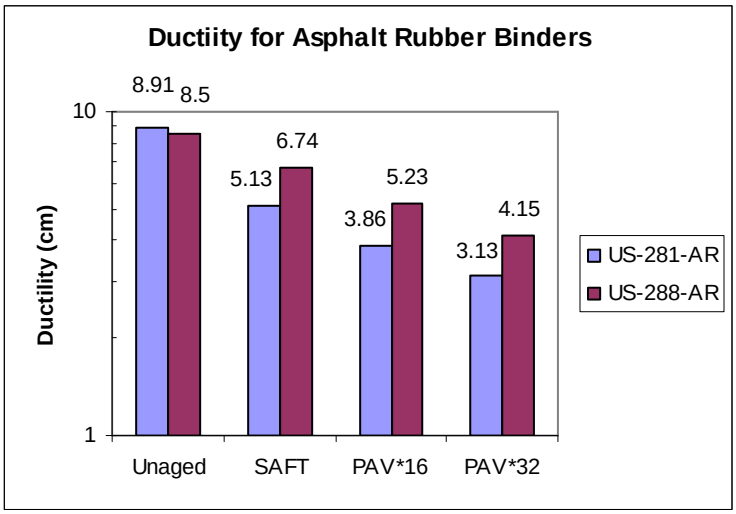

FIGURE 3-4 Ductility for Asphalt Rubber Binders

Force Ductility

The asphalt rubber behaves very differently than an SBS binder when comparing Figure 3-5 to the force ductility plot in Chapter II (Figure 2-14). The three major differences are the AR has a lower elongation ratio, lower stress, and lacks a definitive asphalt modulus and polymer-asphalt modulus. The AR binders at SAFT conditions show an elongation ratio between 2.5 to 3. The SBS binders at SAFT aging have an Elongation ratio between 7 and 11. The AR binder has between 2 to 4 times the elongation ratio. The asphalt rubber's lower elongation ratio translates to the AR not being able to stretch as much under a given load which gives the AR lower ductility values than the SBS.

The AR binders for SAFT, and PAV* aging have lower maximum stress levels than the SBS binders. The AR binders maximum stress levels are between 0.4 and 0.7 MPa, and the SBS binders have maximum stress levels between 1 and 4.5 MPa. The AR binders decrease in stress after they reach the maximum stress unlike the SBS binders which tend to break at the maximum stress level. The AR's lower stress and lack of breaking at the maximum stress is perhaps a sign the rubber in the binder is effective at dissipating stress due to elongation.

Unlike the SBS, AR does not show definitive asphalt and polymer–asphalt moduli. Instead the AR curves at unaged and SAFT aged levels gradually decrease in slope. Although the first part of the curves look similar to an asphalt modulus and the last part of the curves look like an asphalt polymer-modulus, they do not follow the behavior of a modulus which is to have a constant slope over a certain elongation region. The AR PAV* binders show a section which is similar to an asphalt modulus but is not a modulus either. All of the AR binders in Figure 3-5 do not have true moduli; instead, the binder's stress is constantly decreasing. This decrease in stress could be caused by the rubber in the binder and could be another sign the rubber is able to dissipate stress.

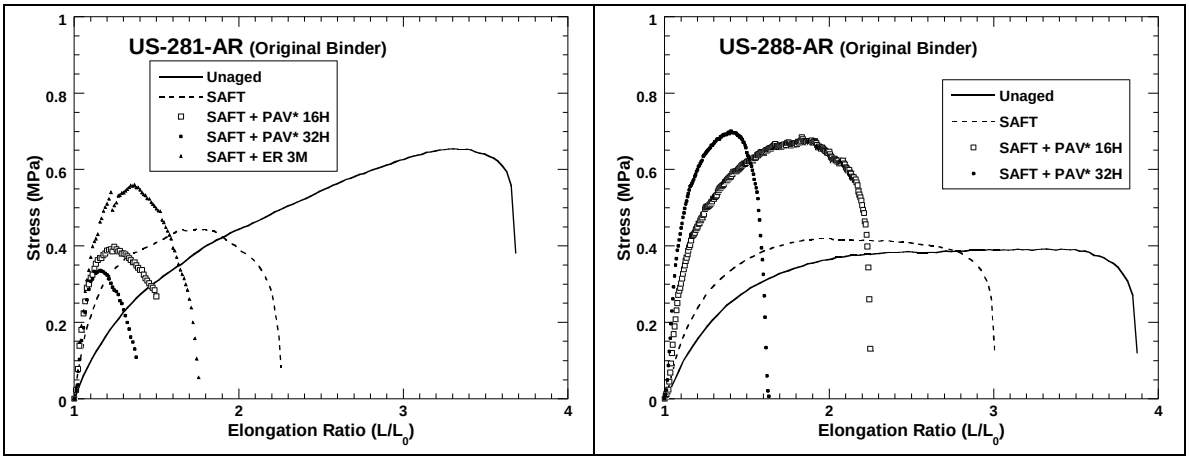

FIGURE 3-5 Asphalt Rubber Force Ductility Curves

SBS and Tire Rubber Binders

The SBS and TR binders perform very differently from the AR binders. In this section the TR and SBS binder rheological properties will be compared to the AR binder rheological properties.

DSR Map

As a binder ages, it moves across the DSR map along a well defined path. Because the binders in Figure 3-6 all follow a similar path, their changes in rheology with aging in general should be similar. TR and AR follow very different paths on the DSR map (Figures 3-6 and 3-1). Their different paths indicate the AR and TR binders perform rheologically completely different.

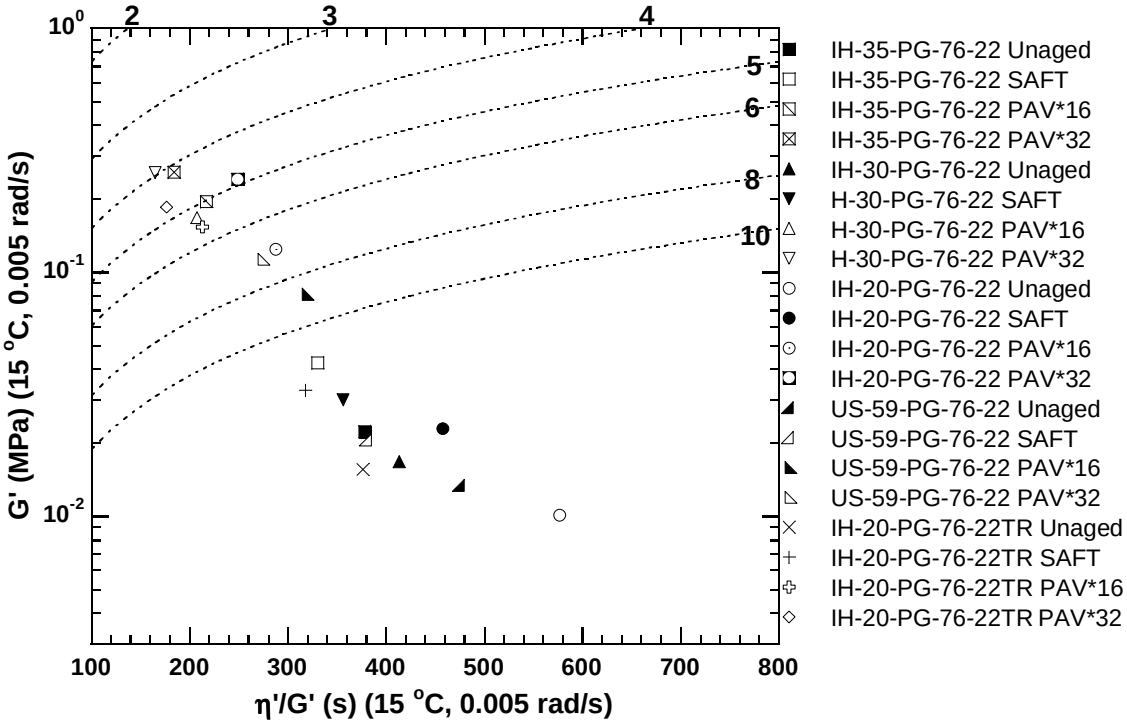

FIGURE 3-6 DSR Map for SBS and TR Binders

Ductility Versus DSR Function

TR binders and SBS binders (Figure 3-7) show an increase in ductility of what would be seen in an unmodified binder. The AR binders in Figure 3-3 show the exact opposite effect. Apparently, SBS and TR improve ductility while the AR does not improve ductility at all and may even decrease it.

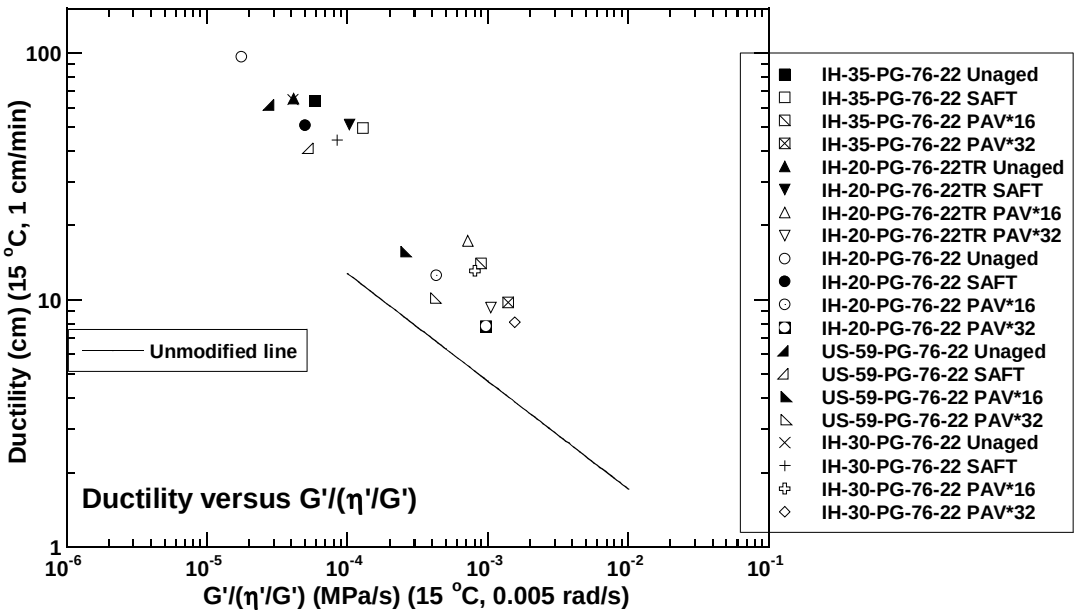

FIGURE 3-7 Ductility Versus DSR Function for SBS and TR Binders

Ductility

Figure 3-8 shows that the SBS binders and TR binders at every aging level have higher ductility values than the AR binders (Figure 3-4). None of the SBS binders and TR binders, unlike the AR binders, have ductility values at PAV* aging levels between 3 and 5 cm, which is good because a ductility of between 3 and 5 cm is a benchmark for possible durability problems (*31*). Because the SBS and TR binders have higher ductility values over the AR binders, the SBS and TR mixtures might be expected to last longer and have fewer problems with cracking.

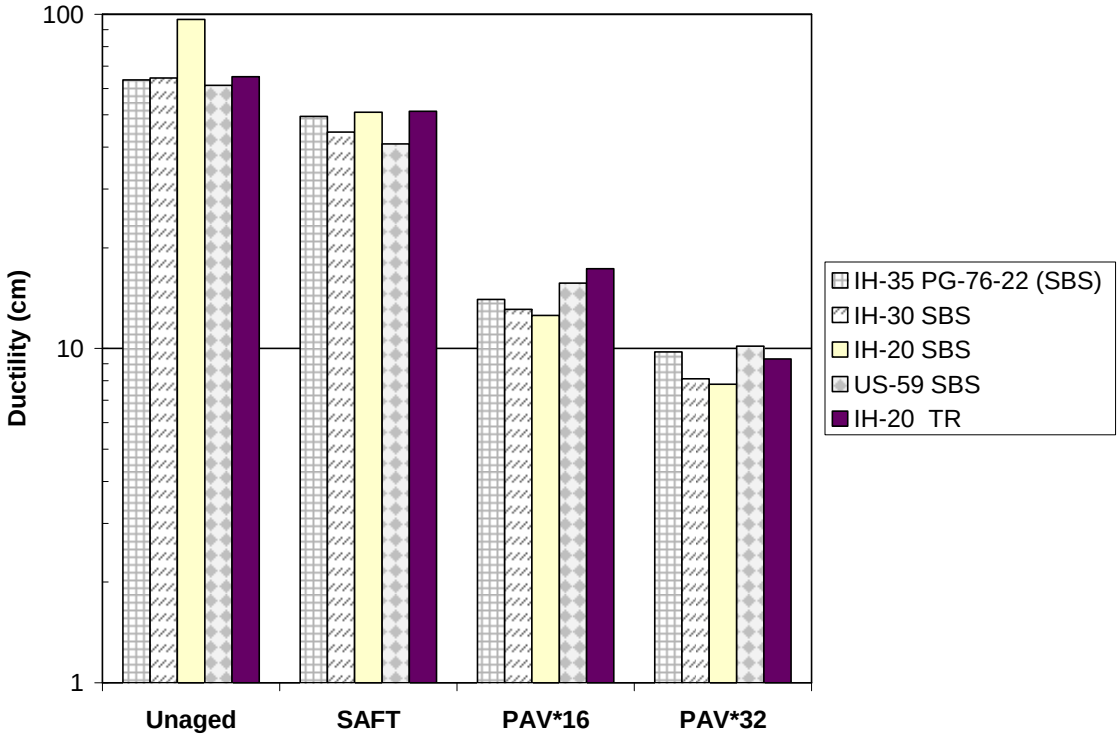

FIGURE 3-8 Ductility of SBS and TR Binders

Force Ductility

Figures 3-9 and Figure 3-10 show similar force ductility curves to those in Chapter II (Figure 2-14). The SBS and TR binders both have polymer-asphalt modulus at unaged and SAFT aging levels. Also, some of the TR binders and SBS binders have a polymer-asphalt modulus at PAV*16, and one binder has a polymer-asphalt modulus at PAV*32. Anyway, both the TR binders and SBS binders of Figure 3-9 and 3-10 have the best force ductility properties in this thesis. Clearly, there is something about these binders which gives them both similar and excellent properties.

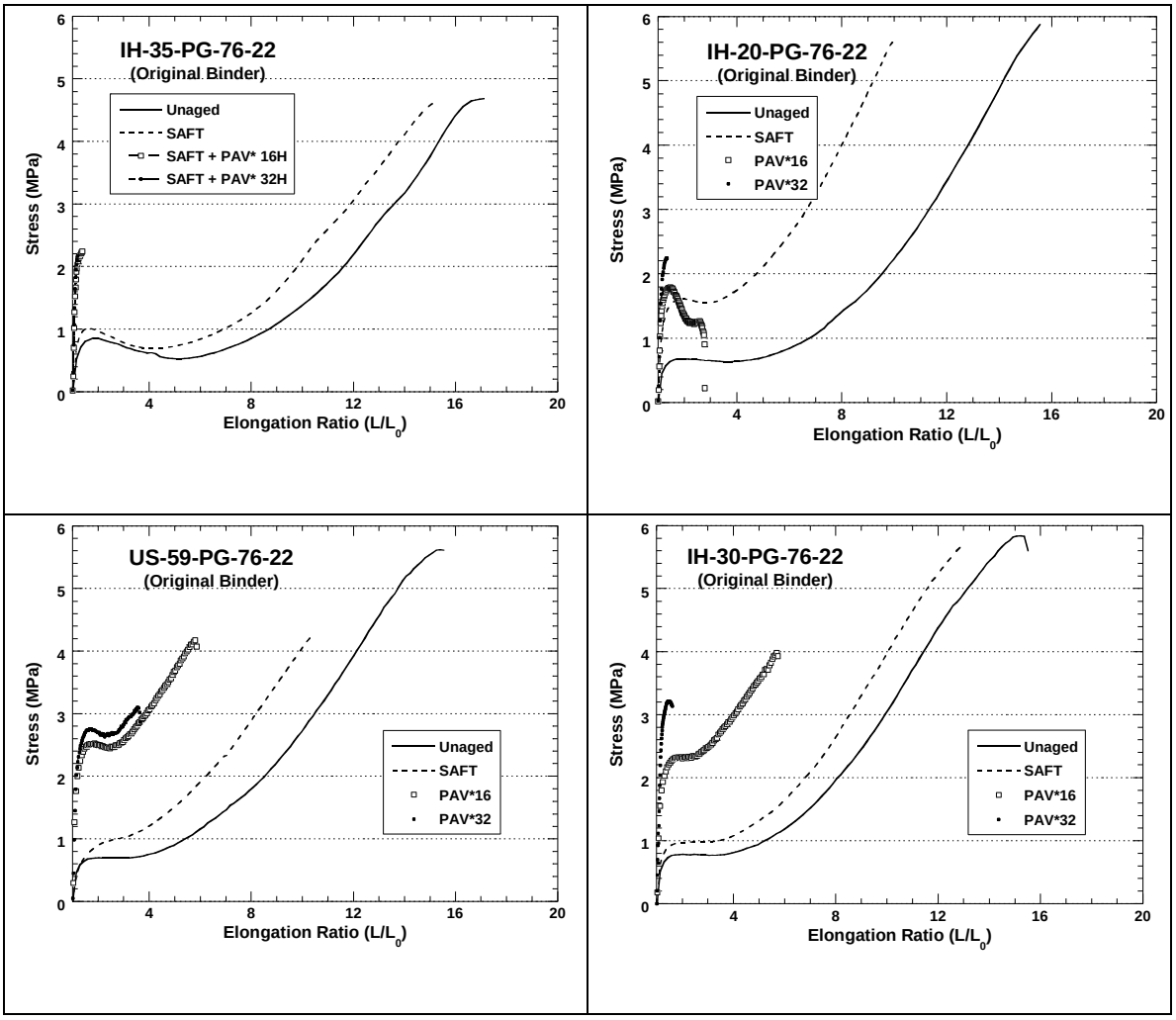

FIGURE 3-9 Force Ductility Data for SBS Binders

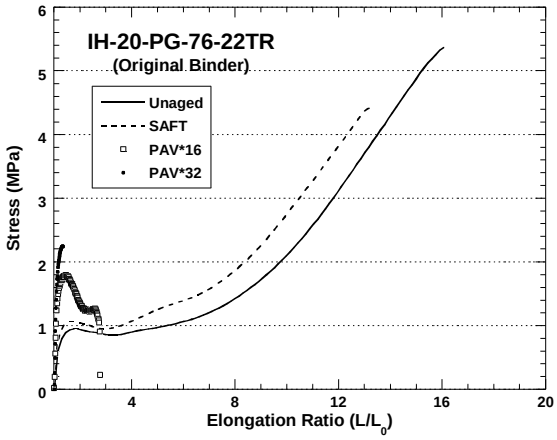

FIGURE 3-10 Force Ductility Data for TR Binders

The SBS binders in Figure 3-9 show very different force ductility properties than those in Figure 2-14. Figure 3-9 typically has greater elongation ratios and greater maximum stress than those in Figure 2-14. Also, the Figure 3-9 binders have polymer-asphalt moduli at PAV* aging but the Figure 2-14 binders do not. Unfortunately, there are no GPC data or microscopy data for the binders in Figure 3-9. But, the force ductility data of Figure 3-9 may possibly tell a story of asphalt binders that have more SBS added and/or have a very structured elastic network initially; however, the actual explanation is not yet known.

CANTABRO TEST DATA

This section discusses a possible relationship between the Cantabro test and a binder's DSR Function. The Cantabro test is important because it gives a simulated measurement of raveling. For PFCs, raveling is the most common source of failure (*5*). To relate the DSR Function to the Cantabro test, there were two options: measure original binders or measure recovered binders from lab/plant mixes. Measuring original binders seemed a better option because an asphalt designer would not need to make a mixture to estimate a PFC mixture's Cantabro loss. Also original binders can be aged

much faster than a mixture which, depending on aging level, can take 3 to 6 months. Using original binders for this relationship is a better option and will hopefully allow an estimate of a mixture's Cantabro Loss.

Before discussing the results of the Cantabro test data, a short explanation is needed about plots of the data that follow. The x axis and y axis show the comparison between G/(η'/G'), DSR function, and percent Cantabro Loss. These axes were chosen to demonstrate a relationship between the percent Cantabro Loss and the DSR function. This relationship is the main purpose of the PFC part of this chapter. The legend has the Asphalts listed as '"Asphalt name" "Binder Age"/ "Mixture Age" "Cantabro'. Also in the legend certain binder ages were paired with specific mixture ages. These pairs are the following: SAFT binder with unaged mixture, PAV*16 binder with 3 month aged mixture and PAV*32 binder with 6 month aged mixture. The PAV* 16 / 3 month mixture and PAV*32 / 6 month mixture were chosen because these ages have been shown to be approximately equivalent for dense mixtures (*22*). Unfortunately, PFCs are believed to age faster than dense mixtures. Although the aging pairs for PAV*16 and PAV*32 may not be exactly equivalent, they should be good enough for an approximation. In the case of the SAFT binder and the unaged mixture, these correspond to two different states for the road production process. SAFT corresponds to the binder coming out of the hot plant, and the unaged mixture corresponds to the mixture after it has been laid on the road and cooled. Although these are two different states, they are assumed to be close enough that they can be used in the comparison in Figure 3-11 and 3-12. Overall, these comparisons should show a relationship between the percent Cantabro loss and the DSR function. But will the relationship be different for plant and lab mixed specimens or similar?

The lab mix lab compacted and the plant mix lab compacted specimens were separated into two different categories on purpose. The lab mix lab compacted specimens were made with specific air void content. The plant mix lab compacted specimens were made with the air void content of the mixture design. Because of the different air void contents, initially these mixtures are discussed in two separate sections. Later, to see if

air void content makes a large difference in this relationship, the two different mixture specimens were combined.

Lab Mix Lab Compacted

Figure 3-11 shows a simple correlation between the Cantabro Loss percentage and the DSR function. The first correlation is the Cantabro Loss percentage increases as the DSR function increases. This correlation seems to follow a straight line that goes from the bottom-left corner to the top-right corner. As the binder and mixture ages, the binder stiffens and the DSR function increases. This increased stiffness in the binder leads to a higher Cantabro Loss which the results in Figure 3-11 show.

Figure 3-11 also shows the DSR Function can be used to predict the Cantabro loss which is a simulated measurement of the degree of raveling of the mixture (*5*). This prediction of the raveling can be made for the mixture at any aging level even before the mixture is made and tested. A good example of where this prediction would be useful is in the case of the US-281-AR mixture. Initially the US-281-AR mixture has very high Cantabro levels compared to the IH-35-PG-76-22 mixture. After aging though these two mixes perform similarly. The DSR function of the binders predicts this behavior and also predicts the Unaged US-281-AR mixture may be above the failure specification of 20 percent Cantabro Loss.

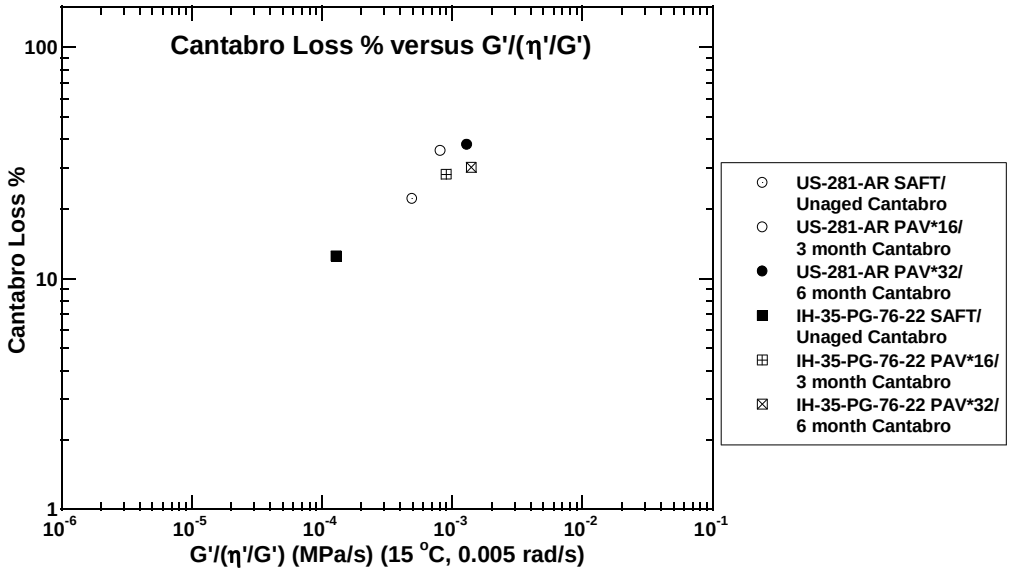

FIGURE 3-11 Cantabro Loss Versus DSR Function for Lab Mix Lab Compacted Specimens

Plant Mix Lab Compacted

The plant mix lab compacted binders displayed in Figure 3-12 show a correlation between the DSR function and the Cantabro loss percentage. The AR data point appears to be an outlier, showing excessive Cantabro Loss (compared to both the SBS and TR materials) for the DSR function value. The big question is whether the data in Figures 3-11 and 3-12 are part of the same correlation.

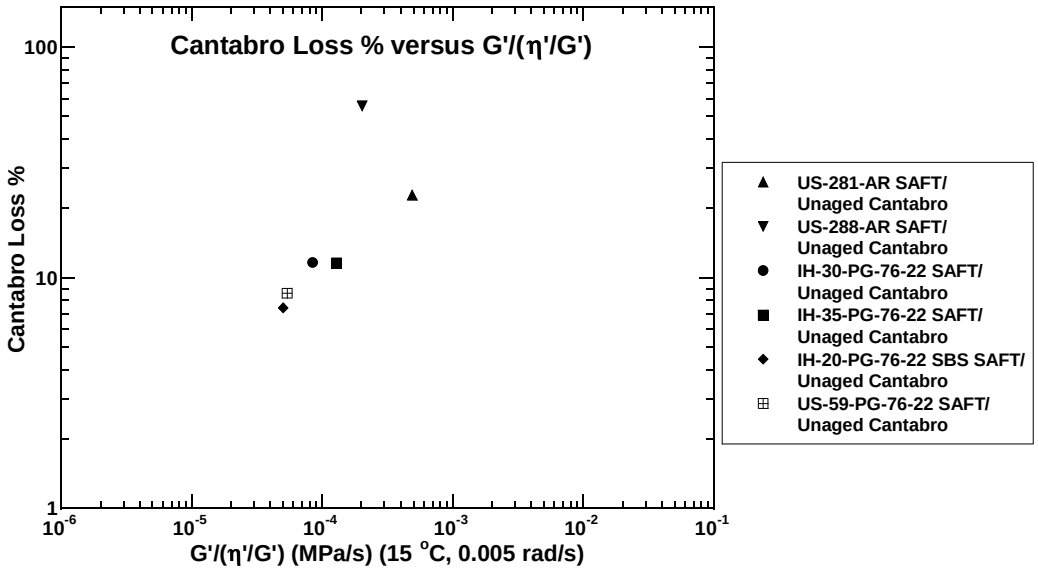

FIGURE 3-12 Cantabro Loss Versus DSR Function for Plant Mix Lab Compacted Specimens

The lab mix and plant mix data (excluding the AR outlier) are combined in Figure 3-13, together with the very good power law correlation ($r^2 = 0.96$). The number of specimens tested is small and more data are needed, but the correlation seems surprisingly good.

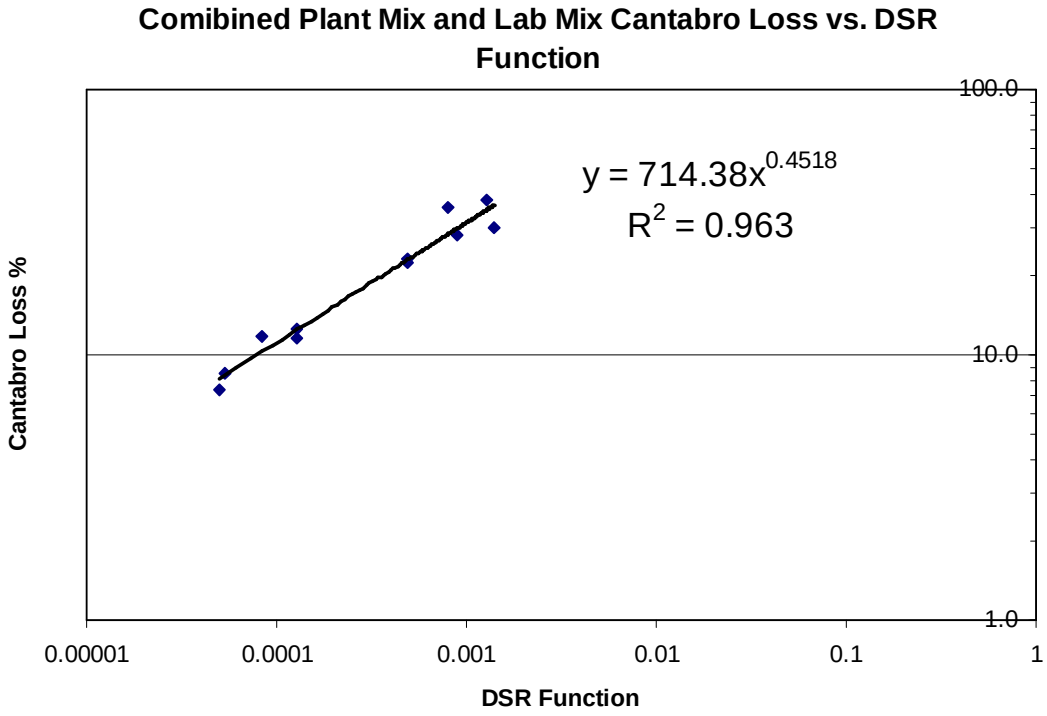

FIGURE 3-13 Combined Plant Mix and Lab Mix Cantabro Loss Versus DSR Function Correlation

CONCLUSIONS

The Conclusions in this chapter are the following:

- Cantabro Loss showed a very good correlation with DSR function independent of whether the mix was lab or plant mix.
- SBS and TR have better ductility and force ductility properties than the AR.
- The AR may be better at relieving stress than TR or SBS.
- The SBS modified asphalts for PFC may have either more SBS or a more structured elastic network than the SBS binder used for dense mixture (binders shown in Chapter II).

- The SBS and TR binder show similar performance based on the force ductility, ductility and DSR map.
- The AR shows completely different rheological behavior than the SBS binder and TR binder.
- Due to the AR's low ductility, AR mixtures may have problems with durability; yet, in this case, ductility may or may not show a relationship with mixture durability.

CHAPTER IV
CONCLUSIONS AND RECOMMENDATIONS

CONCLUSIONS

In Chapter II, polymer morphology was shown to affect both the ductility enhancement and the ductility ratio of the binders. Also The DSR ratio divided by the polymer peak height was related to the ductility ratio of the binders. Because the ductility ratio was related to both polymer morphology and the DSR ratio divided by the polymer peak height, polymer morphology and DSR ratio divided by the polymer peak height should be related also.

In Chapter III DSR correlated well (R^2=0.963) with Cantabro loss percent. This correlation was done without including the US-288-AR specimen which was assumed to be an outlier because of the materials excessive Cantabro loss percent. The correlation also was unaffected by whether or not the mixtures were a lab or plant mixture. The lab mixtures had consistent air voids between 18 to 21 percent but the plant mixtures used the mixture design value for the air void content.

Combining these results from Chapter II and Chapter III, the polymer morphology would affect the DSR Function which would affect the Cantabro Loss percent.

RECOMMENDATIONS

The first and most important recommendation is to take images of the binders from the 5262 project using the fluorescence microscope and get GPC data for the same binders. The images could prove the polymer morphology affects both the rheological properties of the binders and the Cantabro Loss percent. The GPC data can show how much polymer has been added.

The second recommendation is to correlate ductility of the 5262 project binders with durability for the PFC field mixtures. Currently, there is no evidence of a correlation between ductility and PFC mixture durability. Ductility has been shown to be an important indicator for mixture durability problems in dense mixes (23), but for PFC this relationship may not be true.

The third recommendation is to change the procedure of the fluorescence microscopy. For the thesis Fluorescence microscopy images were taken at 50x, 100x, and 200x magnification. Only the images taken at 50x magnification were used for analysis. The 100x and 200x magnification images were not used because problems with the data occurred. At 100x magnification, entire sets of data looked the same possibly due to the top surface slightly melting. At 200 x magnification, melting of the sides occurred for some of the samples. Because of the problems associated with 100x and 200x magnification, all images should be taken at 50x magnification using the fluorescence microscope.

The fourth recommendation is to acquire more data to back up the conclusions of this thesis. Currently, the conclusions lack enough data to be definitive.

REFERENCES

1. Kandhal, Prithvi S. and Rajib B. Mallick. *Design of New-Generation Open-Graded Friction Courses*. Publication NCAT Report No. 99-3, (1999)

2. Watson, Donald, Andrew Johnson, and David Jared. Georgia Department of Transportation's Progress in Open-Graded Friction Course Development. In *Transportation Research Record: Journal of the Transportation Research Board, No. 1616*, Transportation Research Board of the National Academies, Washington, D.C., 1998, pp. 30-33.

3. Watson, Donald E., Kathryn Ann Moore, Kevin Williams, and L. Cooley Jr. Refinement of New-Generation Open-Graded Friction Course Mix Allen Design. In *Transportation Research Record: Journal of the Transportation Research Board, No. 1832*, Transportation Research Board of the National Academies, Washington, D.C., 2003, pp. 78-85.

4. Hassan, Hossam F., Salim Al-Oraimi, and Ramzi Taha. Evaluation of Open-Graded Friction Course Mixtures Containing Cellulose Fibers and Styrene Butadiene Rubber Polymer. *Journal of Materials in Civil Engineering*, Vol. 17, 2005 pp. 416-422.

5. Herrington, Phil, Sheryn Reilly, and Shaun Cook. *Porous Asphalt Durability Test*. Publication Transfund New Zealand Research Report 265, 2005.

6. Ruan, Y., R. R. Davison, and C. J. Glover. An Investigation of Asphalt Durability: Relationships Between Ductility and Rheological Properties for Unmodified Asphalts. *Petroleum Science and Technology*, Vol. 21, pp. 231-254.

7. Lu, Xiaohu and Ulf Isacsson. Chemical and Rheological Characteristics of Styrene-Butadiene-Styrene Polymer-Modified Bitumens. In *Transportation Research Record: Journal of the Transportation Research Board, No. 1661*, Transportation Research Board of the National Academies, Washington, D.C., 1999, pp.83-92.

8. Kuennen, Tom. Polymer Modified Asphalt Comes of Age. *Better Roads Magazine*, 2005, p.1.

9. Wen, Guian, Yong Zhang, Yinxi Zhang, Kang Sun, and Yongzhong Fan. Rheological Characterization of Storage-Stable SBS-modified Asphalts. *Polymer Testing,* Vol. 21, 2002, pp. 295-302.

10. Ho, Rong-ming, Adeyinka Adedeji, David W. Giles, Damian A. Hajduk, Christopher W. Macosko, and Frank S. Bates. Microstructure of Triblock Copolymers in Asphalt Oligomers. *Journal of Polymer Science: Part B: Polymer Physics,* Vol. 35, 1997, pp. 2857-2877.

11. Champion, L., J.-F. Gerard, J.-P. Planche, D. Martin, and D. Anderson. Low Temperature Fracture Properties of Polymer-Modified Asphalts Relationships with the Morphology. *Journal of Materials Science,* Vol. 36, 2001, pp. 451-460.

12. Loeber, L., O. Sutton, J. Morel, J.-M. Valleton and G. Muller. New Direct Observations of Asphalts and Asphalt Binders by Scanning Electron Microscopy and Atomic Force Microscopy. *The Royal Microscopical Society, Journal of Microscopy,* Vol. 182, 1996, pp. 32-39.

13. Champion-Lapalu, L., A. Wilson, G. Fuchs, D. Martin, and J.-P. Planche. Cryo-Scanning Electron Microscopy: A New Tool for Interpretation of Fractures Studies in Bitumen/Polymer Blends. *Energy and Fuels,* Vol. 16, 2002, pp. 143-147.

14. Chen, Jian-Shiuh, Min-Chih Liao, and Ming-Shen Shiah. Asphalt Modified by Styrene-Butadiene-Styrene Triblock Copolymer: Morphology and Model. *Journal of Materials in Civil Engineering*, Vol. 14, 2002, pp. 224-229.

15. Lewandowski, L.H. Polymer Modification of Paving Asphalt Binders. *Rubber Chemistry and Technology,* Vol. 67, 1994, pp. 447-480.

16. Bouldin, M.G., J.H. Collins, and A. Berker. Rheology and Microstructure of Polymer/Asphalt Blends. *Rubber Chemistry and Technology,* Vol. 64, 1991, pp. 577-600.

17. Streitel, S.G. *Luminescent Materials (Fluorescent: Kirk Othmer Encyclopedia of Chemical Technology* 4th Edition. John Wiley and Sons, Inc., New York, 1995.

18. Slavik J. *Fluorescence Microscopy and Fluorescent Probes*. New York, Plenum Press, 1996.

19. Lin, Moon-Sun, Jay M. Chaffin, Meng Liu, C.J. Glover, R.R. Davidson, and J.A. Bullin. The Effect of Asphalt Composition on the Formation of Asphaltenes and Their Contribution to Asphalt Viscosity. *Fuel Science and Technology Int'l.,* Vol. 14, 1996, pp. 139-162.

20. Cortizo, M.S., D.O. Larsen, H. Bianchetto, and J.L. Alessandrini. Effect of the Thermal Degradation of SBS Copolymers During the Ageing of Modified Asphalts. *Polymer Degradation and Stability,* Vol. 86, 2004, pp. 275-282.

21. Glover, Charles J., Richard R. Davidson, Chris H. Domke, Yonghong Ruan, Pramitha Juristyarini, Daniel B. Knorr, and Sung H. Jung. *Development of a New Method for Assessing Asphalt Binder Durability with Field Validation*. Publication FHWA/TX-05/1872-2, Texas Transportation Institute, College Station, TX, 2005.

22. Woo, Won Jun, Edward Ofori-Abebresse, Arif Chowdhury, Jacob Hilbrich, Zachary Kraus, Amy Epps Martin, and Charles Glover. *Polymer Modified Asphalt Durability in Pavements*, Publication FHWA/TX-07/0-4688-1, Texas Transportation Institute, College Station, TX, 2007.

23. GIMP-Downloads. http://www.gimp.org/downloads.

24. Rodriguez, Ferdinand, Claude Cohen, Christopher Ober, and Lynden A. Archer. *Principles of Polymer Systems.* New York, Taylor and Francis, 2003.

25. Read, John and Whiteoak, David. *The Shell Bitumen Handbook* Fifth Edition. London, Thomas Telford Publishing, 2003.

26. Woo, Won Jun, Jacob M. Hillbrich and Charles J. Glover. Polymer Modified Binder Durability Loss with Oxidative Aging: Base Binder Stiffening vs. Polymer Degradation. In *Transportation Research Record: Journal of the Transportation Research Board, No. 1998,* Transportation Research Board of the National Academies, Washington, D.C., 2006, pp. 38-46.

27. Alvarez, Allex E., Amy Epps Martin, Cindy K. Estakhri, Joe W. Button, Zachary Kraus, Nikornpon Prapaitrakul, and Charles J. Glover. *Evaluation and Recommended Improvements for Mix Design of Permeable Friction Courses,*

Report FHWA/TX-08/0-5262-3, Texas Transportation Institute, College Station, TX, 2008.

28. Burr, B. L., C. J. Glover, R. R. Davison, and J. A. Bullin. New Apparatus and Procedure for the Extraction and Recovery of Asphalt Binder from Pavement Mixtures. In *Transportation Research Record: Journal of the Transportation Research Board, No. 1391*, Transportation Research Board of the National Academies, Washington, D.C., pp. 20-29.

29. Way, G. B. ADOT's Use of Crumb Rubber in Asphalt Pavements. http://www.rubberpavements.org/RPA_News/sep97/page3.html.

30. Glover, Charles J., Richard R. Davison, Jerry A. Bullin, Cindy K. Estakhri, Shelly A. Williamson, Travis C. Billiter, Jason F. Chipps, Jay S. Chun, Pramitha Juristyarini, Shauna E. Leicht, and Piyachat Wattanachai. *A Comprehensive Laboratory and Field Study of High-Cure Crumb-Rubber Modified Asphalt Materials*. Publication FHWA/TX-01/1460-1, Texas Transportation Institute, College Station, TX, 2000.

31. Kandhal, P.S. Low-Temperature Ductility in Relation to Pavement Performance. In: Marek, C. R., ed. ASTM STP 628: *Low-Temperature Properties of Bituminous Materials and Compacted Bituminous Paving Mixtures.* Philadelphia, PA: American Society for Testing and Materials, 1977, pp. 95-106.

APPENDIX A

MICROSCOPY IMAGES EXPLAINING HIGH AND LOW STRUCTURE

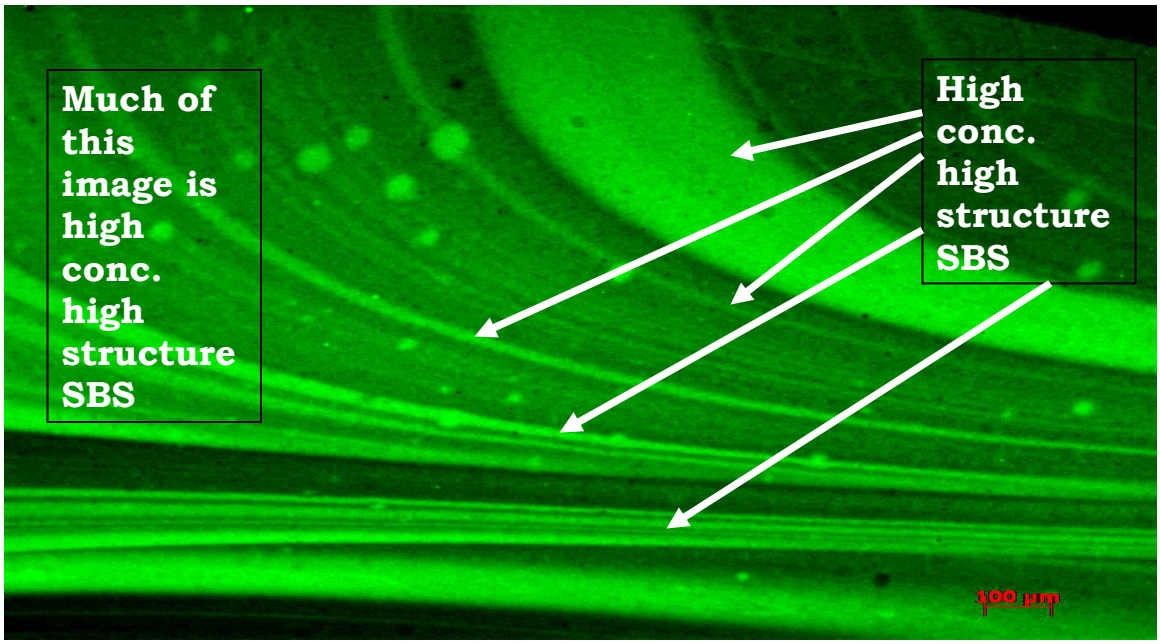

FIGURE A-1 Microscopy Image Showing the High Structure SBS

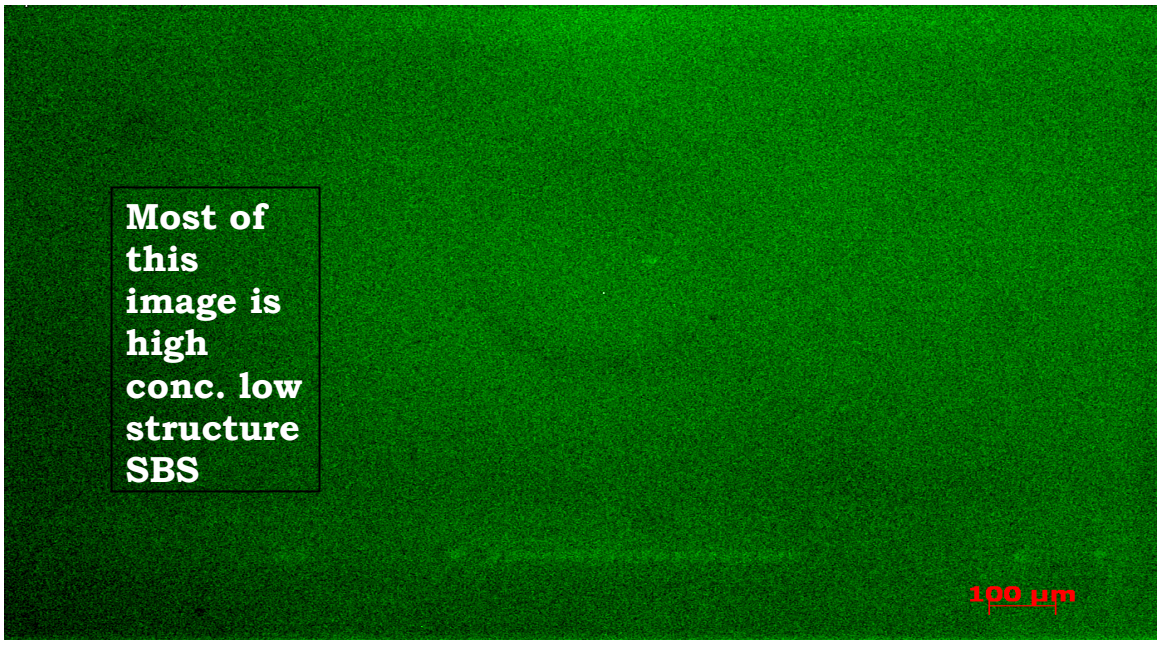

FIGURE A-2 Microscopy Image Showing the Low Structure SBS

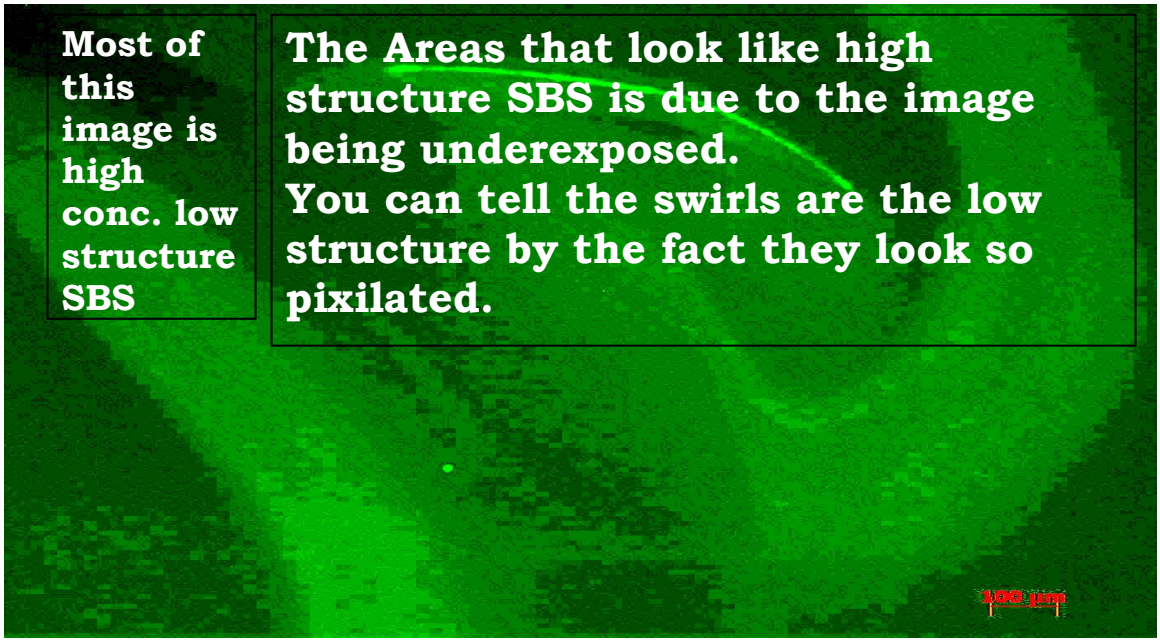

FIGURE A-3 Microscopy Image Showing Low Structure SBS that Looks Like High Structure SBS

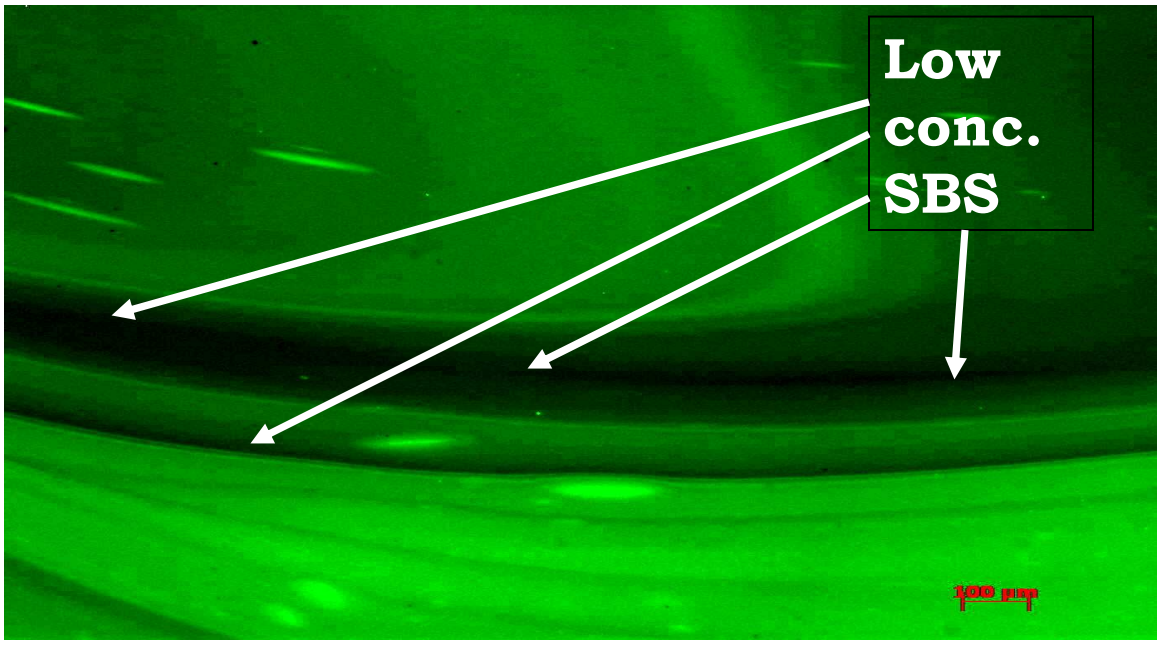

FIGURE A-4 Microscopy Image Showing Low Concentration SBS

APPENDIX B

PFC ASPHALT BINDER RHEOLOGY AND CANTABRO LOSS DATA

VISCOSITY CURVES

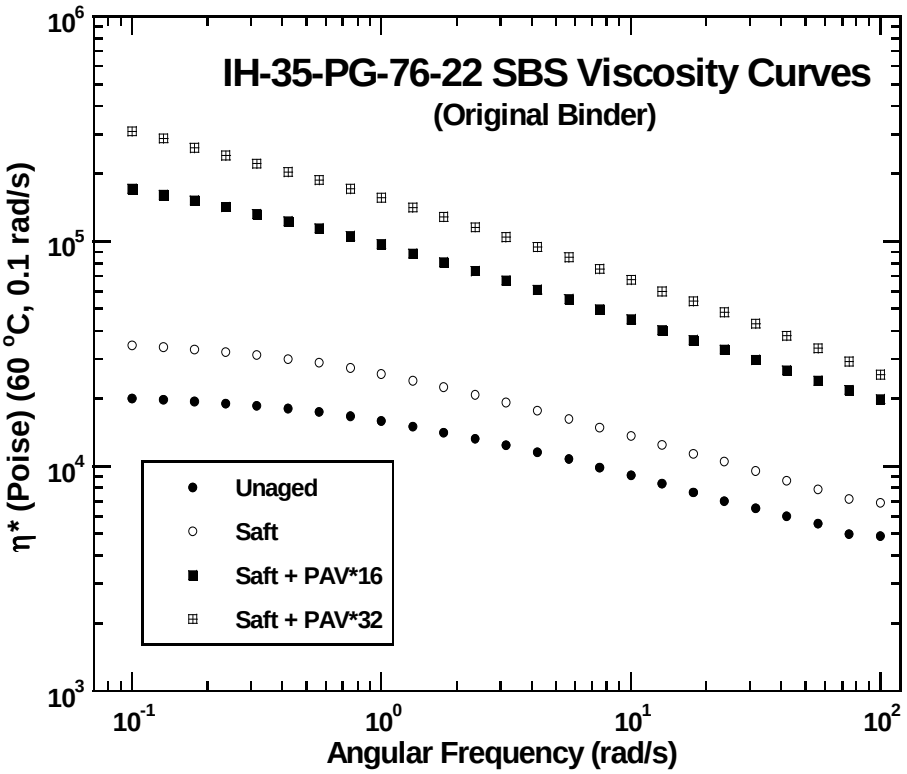

FIGURE B-1 IH-35-PG-76-22 Viscosity Curves

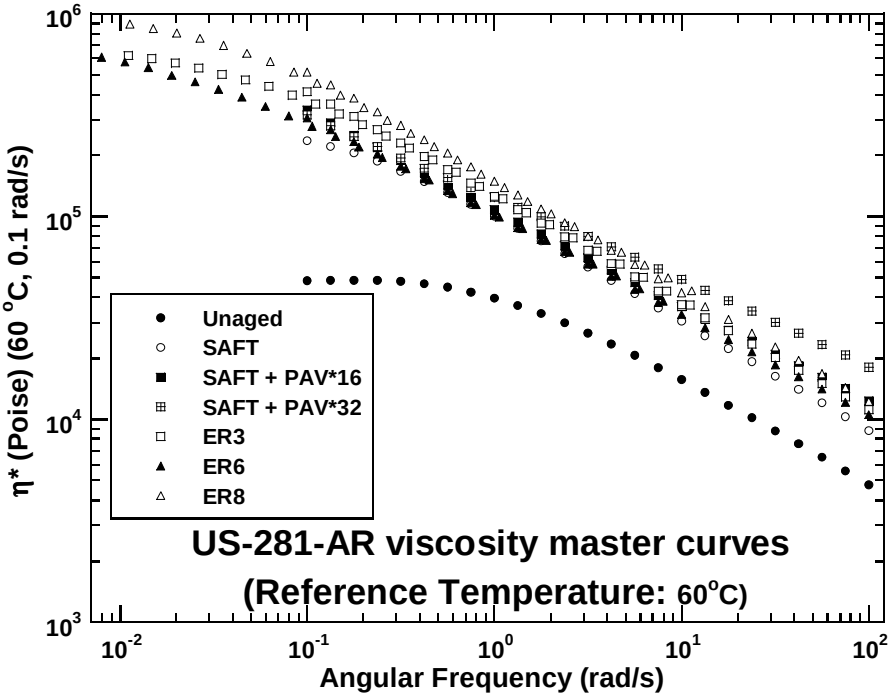

FIGURE B-2 US-281-AR Viscosity Curves

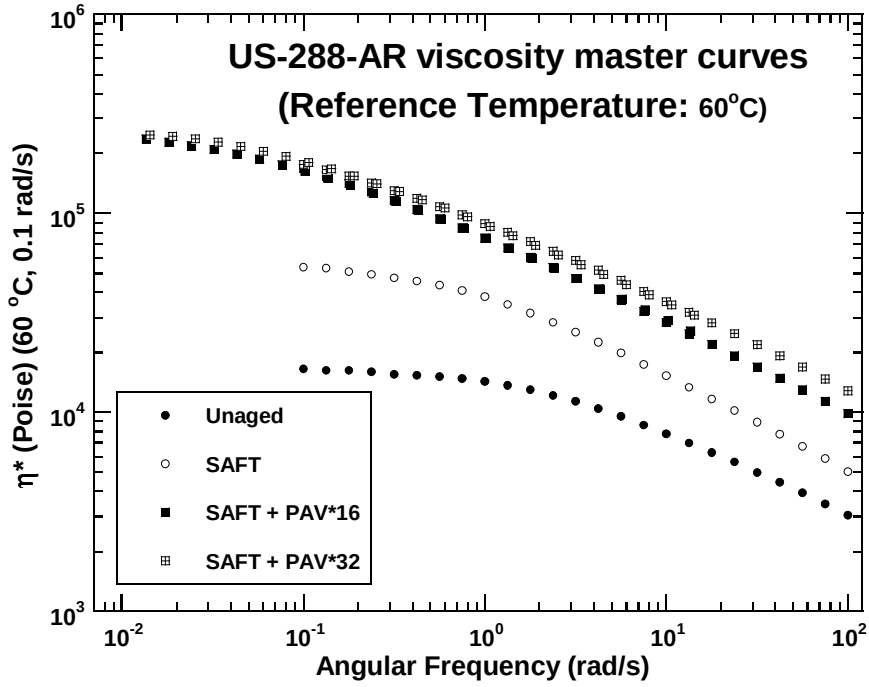

FIGURE B-3 US-288-AR Viscosity Curves

PHASE ANGLE CURVES

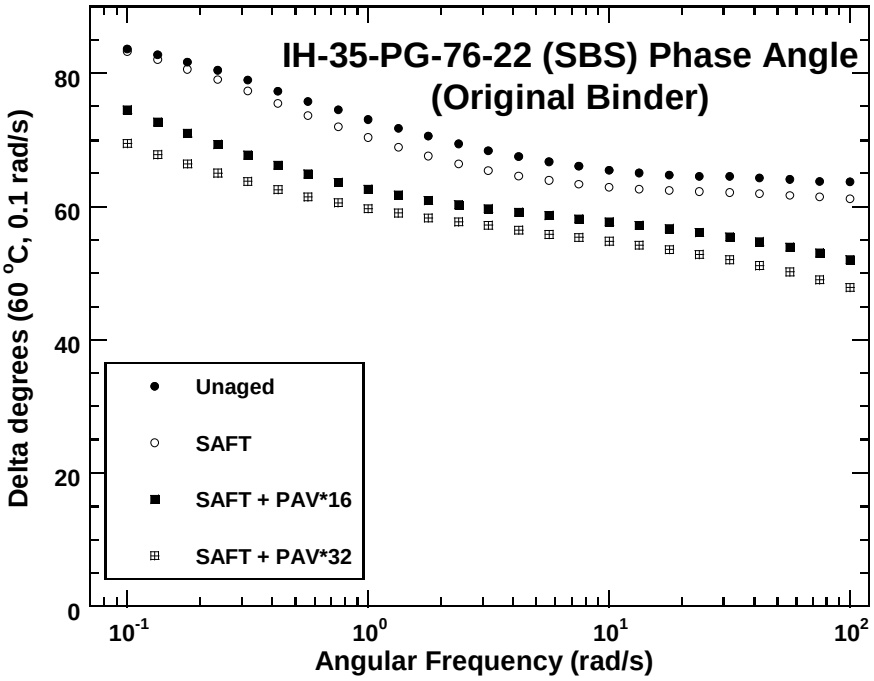

FIGURE B-4 IH-35-PG-76-22 (SBS) Phase Angle Curves

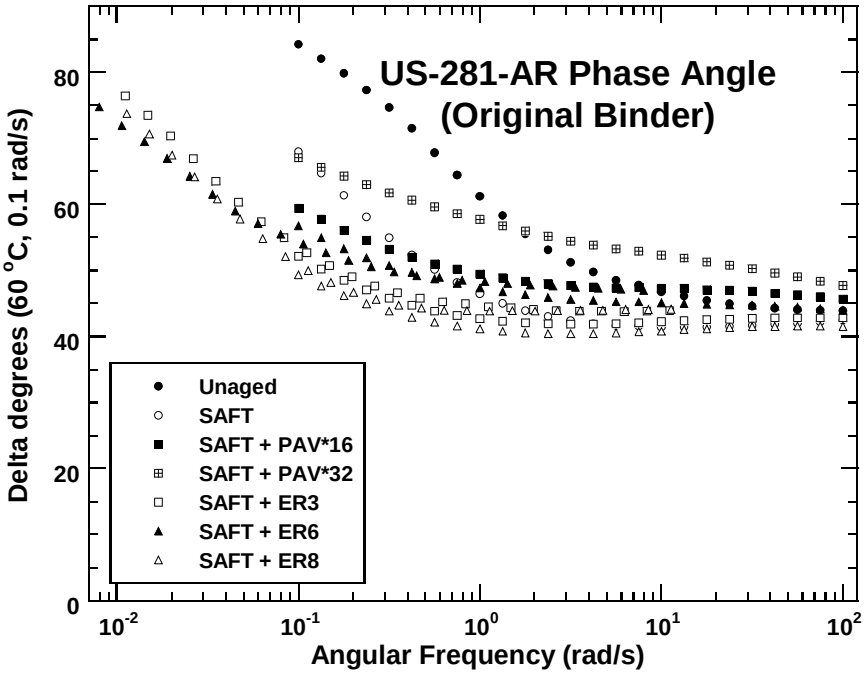

FIGURE B-5 US-281-AR Phase Angle Curves

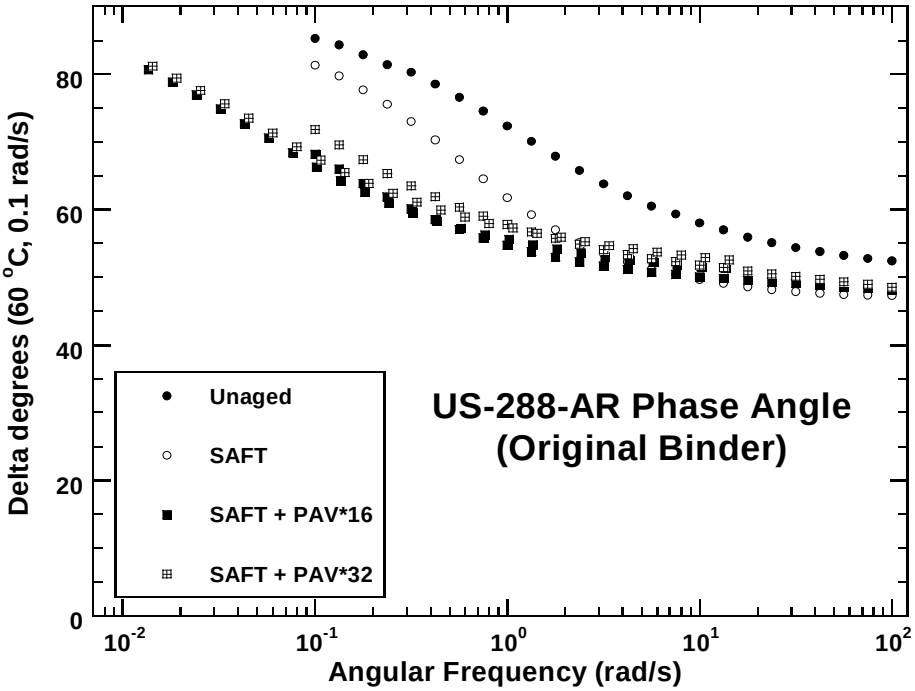

FIGURE B-6 US-288-AR Phase Angle Curves

DSR MAP FOR RECOVERED BINDERS

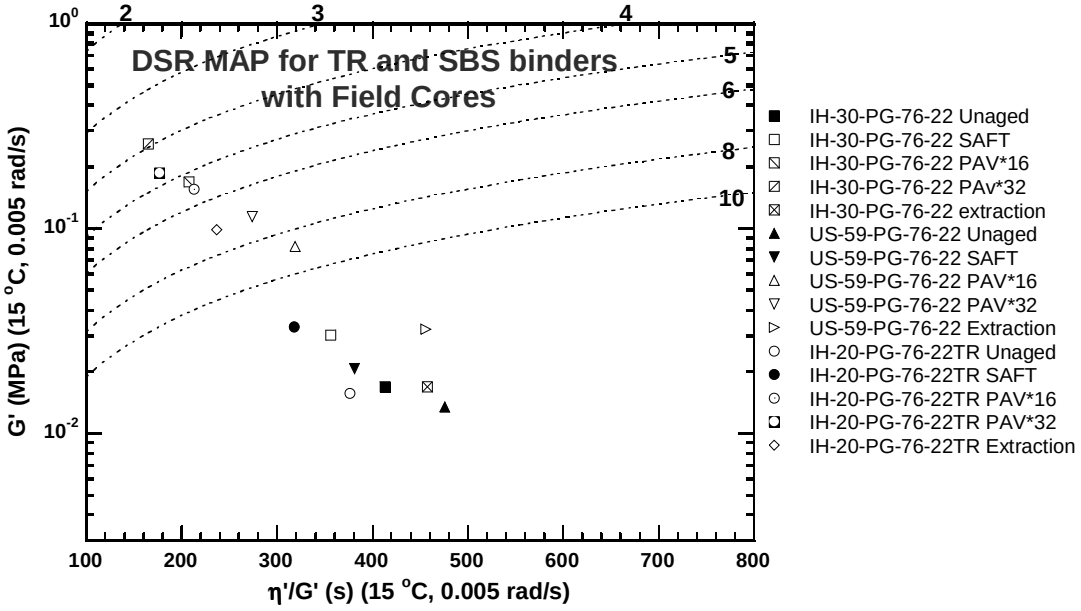

FIGURE B-8 DSR Map for TR and SBS Binders from Field Cores

CANTABRO LOSS DATA

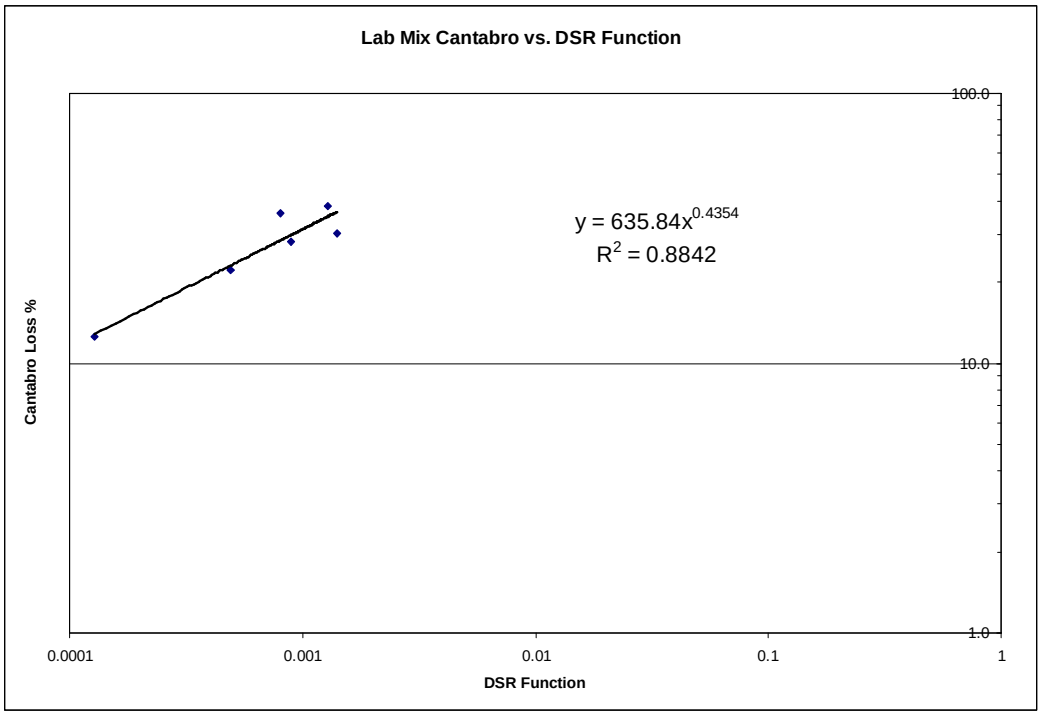

FIGURE B-9 Lab Mix Cantabro Verse DSR Function

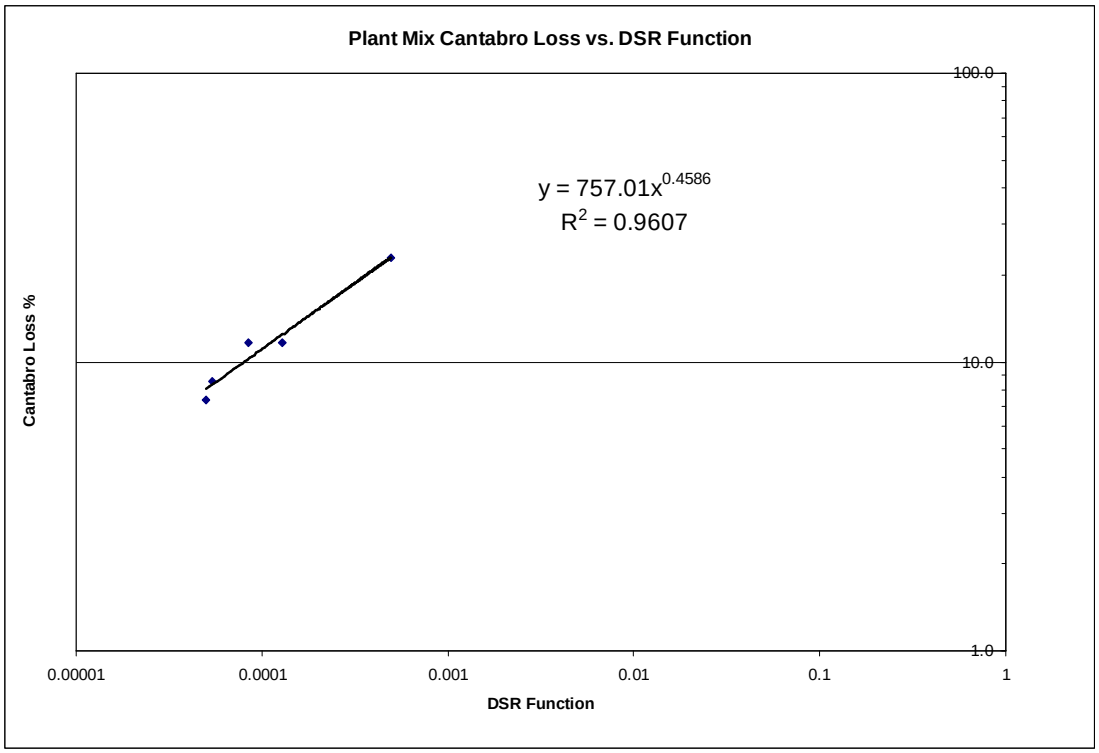

FIGURE B-10 Plant Mix Cantabro Verse DSR Function

VITA

Zachary Rothman Kraus
401 University Oaks Blvd. Apt. 1401, College Station,Texas 77840
zach1@tamu.edu, 404-314-7211

EDUCATION

Texas A&M University College Station , TX
M.S. in Chemical Engineering, GPA: 3.64 Grad: August 2008

Georgia Institute of Technology Atlanta, GA
B.S. in Chemical Engineering, GPA: 3.07 August 2005

RESEARCH EXPERIENCE

Chemical Engineering Dept., Texas A&M University *College Station ,TX*
Research Assistant, Dr. Charles Glover's Research Group *Spring 2006-Present*

- Developed a web based teaching tool for fundamental mass transport.
- Conducted a microscopic analysis of SBS modified Asphalts with a fluorescence microscope.
- Analyzed PFC and Dense mix binder using rheological and chemical experiments.

Chemical Engineering Dept., Georgia Institute of Technology *Atlanta, GA*
Undergrad Research – Dr. Yulin Deng Summer 2004

- Developed a new method of making paper which used less pulp.

Undergrad Research – Dr. Carson Meredith *Fall 2003-Spring 2004*

- Worked on a MC simulation of polymer interactions with ionic compounds.
- Repaired code for AFM microscope to run automatically.

HONORS & AWARDS

9 semesters of Dean's List Fall 2000-Summer 2005

ORGANIZATION

Graduate Student Council Fall 2007-present
Phi Lambda Upsilon-Chemistry honor fraternity Summer 2007-present
Photo Journalist for school yearbook and newspaper Fall 2001-Fall 2002

ACADEMIC PROJECT

AICHE Car Contest Fall 2003-Spring 2004